

Quiescent cancer cells

Three-dimensional cell models for the evaluation
of new therapeutics

Frida Ek

MEDFARM 2022/1765

Dissertation presented at Uppsala University to be publicly examined in Hedstrandsalen, Akademiska sjukhuset ingång 70, Uppsala, Wednesday, 5 October 2022 at 09:00 for the degree of Licentiate of Philosophy. The examination will be conducted in English.

Abstract

Ek, F. 2022. Quiescent cancer cells. Three-dimensional cell models for evaluation of new therapeutics. (Vilande cancerceller. Tredimensionella cellmodeller för utvärdering av nya cancerläkemedel). 59 pp. Uppsala: Uppsala universitet.

Inadequate metabolic conditions in solid tumors lead to the formation of quiescent cancer cells that are suspended in a transient cell cycle arrest. When conditions change, quiescent cancer cells can re-enter the cell cycle and cause recurrence. Drug screening efforts have revealed mitochondrial oxidative phosphorylation as a unique metabolic dependency in quiescent cancer cells. The anthelmintic drug nitazoxanide is an inhibitor of oxidative phosphorylation and preferentially active against quiescent cancer cells in multicellular tumor spheroids.

In this thesis, we employed current and developed new models of quiescent cancer cells and applied live cell imaging for improved preclinical evaluation of cancer drugs in hepatocellular and colorectal carcinoma cell lines. As part of this work, a new assay to measure mitochondrial membrane potential in three-dimensional cell models was developed, an application of the JC-1 assay, and we demonstrated that the preferential activity against quiescent cancer cells of nitazoxanide is shared by two kinase inhibitors: sorafenib and regorafenib. The sensitivity of quiescent cancer cells to nitazoxanide, sorafenib, and regorafenib correlated with the disruption of the mitochondrial membrane potential. Nitazoxanide and sorafenib, in combination, caused an additive decrease in viability, mitochondrial membrane potential, and colony regrowth capacity.

Furthermore, we developed a quiescent hollow fiber assay and implemented an improved analysis using live cell imaging and adenosine triphosphate analysis. Hypoxia and cancer cell quiescence were enriched in hollow fiber macrocapsules over time, and the culture conditions affected nitazoxanide sensitivity. Additionally, we used basement membrane extract gel to support cell growth in hollow fiber macrocapsules and implanted macrocapsules in mice. We observed that the *in vivo* environment was favorable to cell growth. Through this characterization of the quiescent hollow fiber assay, we were able to outline important paths for future research.

Keywords: Cancer, cancer cell quiescence, dormancy, three-dimensional, multicellular tumor spheroids, model development, cancer pharmacology, mitochondria, OXPHOS, colorectal carcinoma, hepatocellular carcinoma

Frida Ek, Department of Medical Sciences, Cancer Pharmacology and Computational Medicine, Akademiska sjukhuset, Uppsala University, SE-75185 Uppsala, Sweden.

© Frida Ek 2022

URN urn:nbn:se:uu:diva-483620 (<http://urn.kb.se/resolve?urn=urn:nbn:se:uu:diva-483620>)

*“All we have to decide is what to do
with the time that is given to us”*

- J.R.R. Tolkien. *The fellowship of the ring.*

List of Papers

- I. **Ek. F**, Blom. K, Selvin. T, Rudfeldt. J, Andersson. C, Senkowski. W, Brechot. C, Nygren. P, Larsson. R, Jarvius. M, Fryknäs. M. (2022) Sorafenib and nitazoxanide disrupt mitochondrial function and inhibit regrowth capacity in three-dimensional models of hepatocellular and colorectal carcinoma. *Scientific Reports*.
- II. **Ek. F**, Selvin. T, Fryknäs. M. The hollow fiber assay for modeling quiescent cancer cells *in vitro* and *in vivo*. *Unpublished manuscript*.

Reprints were made with permission from the publisher.

Additional papers by the author

Handin N, Mickols E, Ölander M, Rudfeldt J, Blom K, **Nyberg F**, Senkowski W, Urdzik J, Maturi V, Fryknäs M, Artursson P. (2021) Conditions for maintenance of hepatocyte differentiation and function in 3D cultures. *iScience*

Niklasson M, Bergström T, Jarvius M, Sundström A, **Nyberg F**, Haglund C, Larsson R, Westermark B, Segerman B, Segerman A. (2019) Mesenchymal transition and increased therapy resistance of glioblastoma cells is related to astrocyte reactivity. *The Journal of Pathology*.

Nazir M, Senkowski W, **Nyberg F**, Blom K, Edqvist PH, Jarvius M, Andersson C, Gustafsson MG, Nygren P, Larsson R, Fryknäs M. (2017) Targeting tumor cells based on Phosphodiesterase 3A expression. *Experimental Cell Research*.

Segerman A, Niklasson M, Haglund C, Bergström T, Jarvius M, Xie Y, Westermark A, Sönmez D, Hermansson A, Kastemar M, Naimaie-Ali Z, **Nyberg F**, Berglund M, Sundström M, Hesselager G, Uhrbom L, Gustafsson M, Larsson R, Fryknäs M, Segerman B, Westermark B. (2016) Clonal Variation in Drug and Radiation Response among Glioma-Initiating Cells Is Linked to Proneural-Mesenchymal Transition. *Cell Reports*.

Contents

Introduction.....	11
Cancer.....	11
Hepatocellular carcinoma.....	11
Colorectal carcinoma.....	12
Tumor metabolism.....	12
Tumor hypoxia.....	13
Cancer cell quiescence and metabolic plasticity.....	13
Quiescence, dormancy, and senescence.....	14
Modeling cancer cell quiescence <i>in vitro</i>	15
Multicellular tumor spheroids (MCTS).....	15
GFP detection simplifies MCTS analysis.....	17
Tumoroids.....	17
<i>In vivo</i> models and the problem with quiescence.....	18
Hollow fiber assay.....	18
Quiescent cancer cells and their response to drug treatment.....	19
Nitazoxanide.....	19
Observations of nitazoxanide's efficacy in MCTS <i>in vitro</i>	20
Culture conditions determine the drug response.....	22
Sorafenib and regorafenib in advanced stages of HCC.....	23
Aim.....	25
Paper I.....	25
Paper II.....	25
Methods.....	26
Cell culture.....	26
Multicellular tumor spheroid culture and growth.....	26
Monolayer cell seeding.....	27
Patient cell preparation.....	27
Tumoroid culture.....	27
Preparation and cell culture inside hollow fiber macrocapsules.....	28
Galactose experiments.....	29
Drug treatment.....	30
Live cell imaging.....	30
ATP-assay.....	30
The fluorometric cytotoxicity assay.....	31

MTT assay	31
Immunohistochemistry	31
Clonogenic assay	31
JC-1 2D.....	32
JC-1 3D.....	32
CellTiterGlo 3D.....	33
Library of Integrated Network-Based Cellular Signatures-analysis ...	33
Statistics.....	33
Results and Discussion	34
Paper I	34
Sorafenib and nitazoxanide disrupt mitochondrial function and inhibit regrowth capacity in three-dimensional models of hepatocellular and colorectal carcinoma	34
Results	34
Sorafenib shares similarities with OXPHOS inhibitors	34
Sorafenib, regorafenib, and nitazoxanide kill quiescent cancer cells in 3D cell models.....	34
Sorafenib, regorafenib, and nitazoxanide disrupt mitochondrial function in a new 3D assay.....	35
Colony regrowth potential is decreased by increased sorafenib and nitazoxanide exposure duration.....	35
Sorafenib and nitazoxanide show great promise in combination.....	36
Discussion	36
Conclusions from Paper I	39
Paper II.....	40
The hollow fiber assay for modeling quiescent cancer cells <i>in vitro</i> and <i>in vivo</i>	40
Results	40
Large 3D structures need space and time to develop	40
Hypoxia and quiescence are enriched in hollow fiber macrocapsules over time.....	40
Quiescent hollow fiber macrocapsules are sensitized to the OXPHOS inhibitor nitazoxanide.....	41
Viability assays and BME-gel as means of method development	41
<i>In vivo</i> studies.....	42
Discussion	43
Conclusions from Paper II.....	46
Concluding remarks and future perspectives.....	47
Acknowledgements.....	50
References.....	52

Abbreviations

2D	Two-dimensional
3D	Three-dimensional
5-FU	5- fluorouracil
ATP	Adenosine triphosphate
BME	Basement membrane extract
CV	Control value
CoA	Acetyl coenzyme A
CRC	Colorectal carcinoma
DMEM	Dulbecco's modified eagle medium
DMSO	Dimethyl sulfoxide
DNA	Deoxyribonucleic acid
EGF	Epidermal growth factor
FCCP	Carbonyl cyanide-p-trifluoromethoxyphenylhydrazone
FDA	Fluorescein diacetate
FDA	U.S food and drug administration
FMCA	Fluorometric microculture cytotoxicity assay
GFP	Green fluorescent protein
HCC	Hepatocellular carcinoma
HFA	Hollow fiber assay
HIF-1	Hypoxia inducible factor 1
HIF-1 α / β	Hypoxia inducible factor 1 alpha/beta
IC50	Half-maximal inhibitory concentration
IHC	Immunohistochemistry
LINCS	Library of Integrated Network-Based Cellular Signatures
MCTS	Multicellular tumor spheroids
MMP/ ψ m	Mitochondrial membrane potential
MTT	3-[4,5-dimethylthiazol-2-yl]-2,5-diphenyltetrazolium bromide
NCI	National cancer institute (U.S)
OXPHOS	Oxidative phosphorylation
PBS	Phosphate buffered saline
PDH	Pyruvate dehydrogenase

PVDF	Polyvinylidene fluoride
SD	Standard deviation
SEM	Standard error of the mead
TACE	Transarterial chemoembolization
TCA	Tricarboxylic acid
TME	Tumor microenvironment

Introduction

Cancer

Cancer is a collection of diseases in which cells gain limitless replicative potential, leading to uncontrolled proliferation. Uncontrolled proliferation of cells leads to invasion into nearby tissues, and cancer cells have the capacity to spread to distant organs via metastatic spread (Hanahan and Weinberg, 2000). Each type of cancer has a unique genetic makeup due to the high mutation rate of malignant cells; however, it can be divided into various types based on its origin—carcinoma, sarcoma, leukemia, lymphoma, and myeloma. Carcinoma is the most common type of cancer and originates from epithelial tissue, such as the skin or lining of internal organs (“What Is Cancer?,” 2007).

Due to the sustained proliferation of cancer cells, treatment options mainly target proliferation (Wenzel et al., 2014). The three main pillars of cancer therapy are surgery, radiotherapy, and chemotherapy, and they aim to remove and kill the rapidly proliferating tumor mass. Recently, there have been promising advances in immunotherapy, targeted therapy, hormone therapy, stem cell transplantation, and precision medicine (“Types of Cancer Treatment - National Cancer Institute,” 2017).

Hepatocellular carcinoma

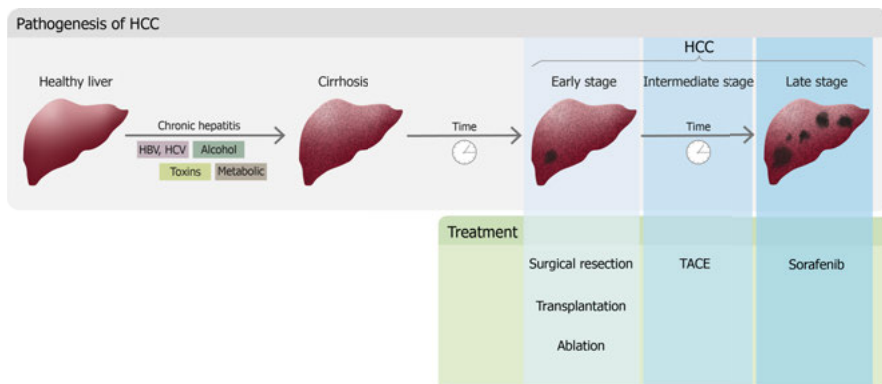


Figure 1. Pathogenesis and treatment of hepatocellular carcinoma.

Hepatocellular carcinoma (HCC) is the fourth leading cause of cancer-related deaths globally and the most common primary liver cancer (Yang et al., 2019). In HCC, the life expectancy is <2 years (Kung-Chun Chiu et al., 2019). Chronic viral hepatitis C and B infections are the most important risk factors and cause 80% of HCC cases globally. Other risk factors include alcoholism and exposure to toxins, especially aflatoxin and aristolochic acid. The disease onset varies geographically, and in Europe, North America, and Japan, the onset occurs above the age of 60. In African countries and parts of Asia, the onset occurs much earlier—between 30 and 60 years of age (Yang et al., 2019).

Treatment options for early-stage HCC include local ablation, surgical resection, and liver transplantation. Patients suitable for surgical resection have no significant portal hypertension and do not display symptoms such as ascites of the abdomen, esophageal varices, and a low platelet count. Liver transplantation is a more drastic treatment option for patients with local tumors and affected liver function, which precludes surgical resection. The advantage of transplantation is the removal of not only the tumor but also the surrounding cirrhotic tissue, which can cause relapse due to progressed carcinogenesis (Yang et al., 2019). However, only a minority of HCC patients are eligible for these treatment options, since the disease is detected at later stages—when liver function is compromised and the disease has spread (Kung-Chun Chiu et al., 2019). HCC is a tumor type characterized by heterogeneity at the pathophysiological and molecular levels as well as hypoxic avascular areas (Calderaro et al., 2017).

Colorectal carcinoma

Colorectal carcinoma (CRC) is one of the most common types of cancer. The numbers of CRC cases and resultant deaths have been increasing each year (Sawicki et al., 2021); 30% of CRC cases are familial or hereditary, and in 70% of sporadic cases, lifestyle factors play a significant role (Mármol et al., 2017).

Tumor metabolism

In normal, slowly proliferating cells, glucose is absorbed and metabolized to pyruvate in the cytoplasm, generating two adenosine triphosphate (ATP) molecules. Pyruvate is oxidized into acetyl coenzyme A (CoA) by the pyruvate dehydrogenase complex (PDH). Acetyl CoA fuels the tricarboxylic acid (TCA) cycle, generating mainly nicotinamide adenine dinucleotide (NADH); thereafter, high-yield ATP is generated from OXPHOS (Lu et al., 2015). Proliferation is an energy-consuming activity because mitosis entails doubling of the total cellular biomass. In proliferating cancer cells, the uptake

of glucose and the rate of glycolysis increase drastically. High glucose consumption generates sufficient ATP to sustain the cancer cells. Even though more ATP would have been produced through OXPHOS, metabolism economy is not an issue in a nutrient-rich microenvironment, such as a highly vascularized tumor tissue (Vander Heiden et al., 2009).

Tumor hypoxia

Due to the fast proliferation rate of cancer cells, malignant tumors outgrow their blood vessels, and the existing vessels are structurally and functionally abnormal, causing turbulent blood flow and less efficient blood supply. This variability in vascularity causes steep gradients at radial distances from nutritious blood flow and lower oxygen levels at increasing distances from the vessel. Cells further away than 70 μ m from the blood supply become hypoxic, and poor perfusion in the tumor can aggravate hypoxia. Due to the gradients of oxygen supply and heterogeneous cancer cell metabolism, hypoxia spreads unevenly in the tumor tissue (Semenza, 2013). Unlike normal tissues, where hypoxic conditions are transient, hypoxia in malignant tumors is often chronic (Vaupel et al., 2004). Hypoxia ($pO_2 \leq 10$ mm Hg) is present in most rapidly growing tumors and is associated with a more aggressive phenotype (Semenza, 2013).

In hypoxic conditions, the genetic expression profile of cancer cells changes, and since the hypoxia is chronic, the hypoxia-induced expression pattern is more stable compared with that of transient hypoxia in normal tissues. Hypoxia-inducible factor 1 (HIF-1) is one of the most important transcription factors induced in hypoxic conditions. HIF-1 upregulation leads to a phenotypic switch in affected cells, leading to increased glycolysis, energy preservation, apoptosis induction, and elevation of hemoglobin levels, among other things (Vaupel et al., 2004). HIF-1 has two subunits: HIF-1 α , which is O₂-regulated, and HIF-1 β , which is constitutively expressed.

Increased HIF-1 α expression is associated with poor prognosis in many types of cancers, including colon and liver cancer (Semenza, 2013). One of the most important functions of HIF-1 is to induce angiogenesis, that is, to recruit new blood vessel formation (Vaupel et al., 2004). Malignant tumors with more widespread hypoxia, or even anoxia, have higher metastatic and invasive potential and decreased sensitivity to radiation and chemotherapy (Vaupel et al., 2004).

Cancer cell quiescence and metabolic plasticity

Due to imbalances between the supply and demand of oxygen, the cancer microenvironment is metabolically heterogeneous. Hypoxia is not the only microenvironmental inadequacy that avascular tumor areas and micrometastases endure (Semenza, 2013). The pH in a malignant tumor mass

is lower (5.8–7.6) than that in normal tissues (7.2–7.5); moreover, the glucose level in malignant tumor mass is 3–10 times lower than that in normal tissues, mainly due to the high glucose consumption of rapidly proliferating cells (Birsoy et al., 2014; Sutherland, 1988). In a microenvironment inadequate for proliferation, with hypoxia, nutrient deprivation, acidosis, and lack of growth factors, metabolic plasticity gives rise to quiescent cancer cells (Porporato et al., 2018; Viale et al., 2015).

Quiescent cancer cells are cancer cells that have temporarily exited the cell cycle and have undergone proliferation arrest. Due to low glycolytic activity and slow or absent proliferation, quiescent cancer cell populations can remain clinically undetectable for a long time before entering a phase of rapid proliferation. This applies not only to quiescent cells in tumors but also to micrometastasis, where angiogenesis has not yet occurred (Holmgren et al., 1995). The reactivation of quiescent cancer cells can cause relapse and lethal secondary tumors. To find new therapies targeting quiescent cancer cells, cell models of quiescence are needed.

Quiescence, dormancy, and senescence

The notion of non-proliferating cancer cells is not exactly new. In 1934, when Rupert Willis discovered that a patient with no local recurrence suffered from mortal secondary tumors nonetheless, he stated, “The neoplastic cells must have lain dormant in the tissues in which they were arrested” (Willis, 1934). In 1954, Geoffrey Hadfield studied late recurrence and suggested that “When the interval is prolonged to six years or more it seems impossible to escape the conclusion that cells of the dormant growth are in a state of temporary mitotic arrest” (Hadfield, 1954).

Since then, several different terms have been used interchangeably to describe the same or completely different phenomena. Dormant cancer cells and quiescent cancer cells are the same thing: non-proliferating cancer cells that have temporarily exited the cell cycle. This can also be specified as cellular dormancy or cellular quiescence. Dormancy can also be used to describe arrested growth of the entire tumor when the rate of proliferation and cell death is at equilibrium. This is described as tumor mass dormancy, and it is not the same as cellular dormancy/quiescence (Endo and Inoue, 2019). Hereafter, I will use “quiescence” to refer to cellular quiescence and nothing else.

Quiescence and senescence are sometimes used synonymously when both cell types have exited the cell cycle. Senescent cells, however, are irreversibly suspended in growth arrest and will eventually die, whereas quiescent cells “have lost none of their former capacity to grow rapidly and infiltrate widely” (Hadfield, 1954) and will re-enter the cell cycle when conditions change. Quiescence occurs in metabolically inadequate microenvironments, whereas

senescence occurs due to aging and extended DNA damage. Therefore, senescent cells cannot cause cancer recurrence and metastasis.

Cancer stem cells are sometimes confused with quiescent cancer cells as well, and they share similarities by often being slow-cycling or in reversible cell cycle arrest. However, cancer stem cells have stemness and a differentiation capacity that quiescent cancer cells do not (Phan and Croucher, 2020). Cancer stem cells do not necessarily have to be quiescent, but they can often be in a quiescent state (Nik Nabil et al., 2021).

Modeling cancer cell quiescence *in vitro*

Two-dimensional (2D) cell cultures, also known as monolayer cell cultures, are the most common and traditionally used model for anticancer therapies *in vitro*. Cells grown in a 2D culture have access to a homogeneous supply of nutrients, oxygen, and supplements, and they grow polarized with attachment to the cell culture vessel. Findings from 2D cell cultures poorly recapitulate the situation *in vivo*, and more relevant cell models need to be used in drug screening and evaluation of cancer therapeutics (Tatullo et al., 2020). There are different types of 3D cell models with different levels of heterogeneity. The most homogeneous and therefore suitable model for high-throughput screening and assays where the variation is preferably low is perhaps multicellular tumor spheroids (MCTS).

Multicellular tumor spheroids (MCTS)

MCTS show many characteristics with tumors *in vivo*. MCTS comprise cells from immortalized cell lines that are allowed to self-assemble into aggregates (Zanoni et al., 2016). In the spheroidization phase, when MCTS are formed into dense, spherical structures from loose aggregates, the growth kinetics are similar to those during the formation of tumors *in vivo*. At the beginning of the spheroidization phase, most cells continue to proliferate; however, as cell connections become stronger and the expression of cell adhesion molecules increases, the proportion of proliferating cells decreases and is replaced by quiescent cells (Karlsson et al., 2012a; Sutherland, 1988). At the end of the spheroidization phase, diffusion limitations arise due to cellular density and increased interstitial fluid pressure, and a steady state of MCTS growth occurs (Zanoni et al., 2016). These diffusion limitations cause steep gradients of oxygen and nutrients to form outside MCTS, similar to gradients formed at radial distances from blood vessels in tumors.

The metabolism of MCTS can be altered by changing cell culture conditions. The amount of proliferation within MCTS can be increased via frequent medium changes, which more quickly creates proliferating MCTS that lack a large proportion of quiescent cells. If the medium is not changed during the spheroidization phase (7 days), the medium becomes depleted of

nutrients with acidosis and low glucose levels. We call this conditioned media, and the MCTS grown in conditioned media are highly quiescent (Senkowski et al., 2016).

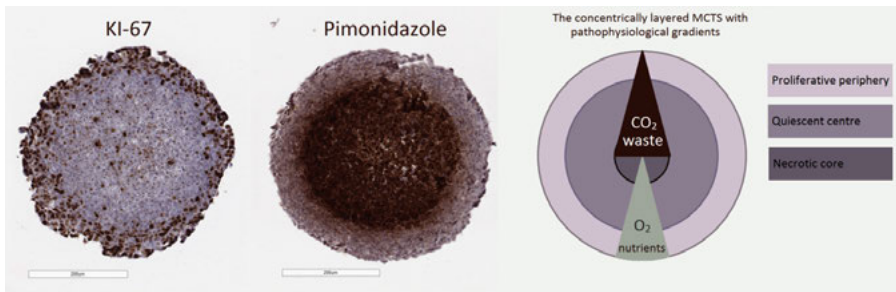


Figure 2. Immunohistochemistry (IHC) IHC of seven-day quiescent MCTS. KI-67 positivity in the periphery of MCTS indicates the presence of proliferating cells. Pimonidazole, a hypoxia marker, is positive in the center of the MCTS. Concentric layers are formed due to the gradients of oxygen and nutrients caused by the diffusion limitations. Accumulation of CO₂, lactate, and waste from the center and outward forms a necrotic core in older MCTS.

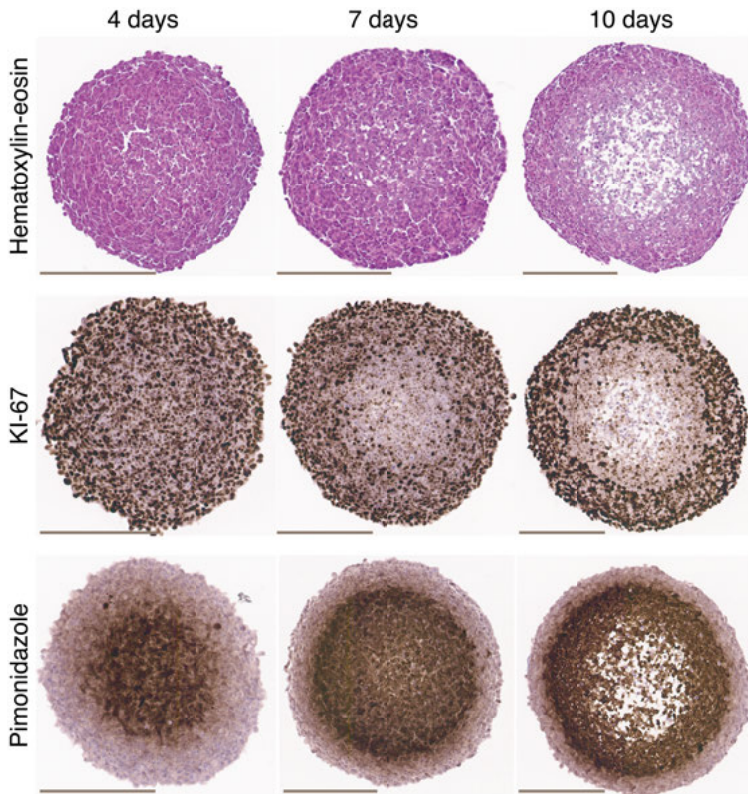


Figure 3. Spheroid growth over time (4, 7, and 10 days) with hematoxylin-eosin staining, ki-67 (proliferation marker), and pimonidazole (hypoxia marker).

GFP detection simplifies MCTS analysis

HCT116-GFP has a constitutive expression of green fluorescent protein (GFP), which is a sensitive marker of cell viability and has been used as a viability readout for high-throughput screening in MCTS (Senkowski et al., 2015). The GFP assay has been compared with the laborious and time-consuming fluorescein diacetate (FDA)-based viability assay FMCA (Lindhagen et al., 2008), and the GFP assay turned out to be even more sensitive to the early signs of cell death (Karlsson et al., 2012b).

Tumoroids

Patient tumor cells grown *in vitro* and treated with chemotherapy have been used to predict the sensitivity of the patient *in vivo* (Nygren and Larsson, 2008). If patient cells are grown in a 3D culture as tumoroids, they survive longer, can be expanded, and are still pathophysiologically and genetically similar to the original patient tumor (Finnberg et al., 2017; Tatullo et al.,

2020). Tumoroids are often grown in some type of hydrogel-based matrices with higher viscosity to allow for easier cell–cell connections and prevent attachment to cell culture vessels, as observed in a monolayer cell culture. However, there are other methods, such as hanging drop methods, rotation in bioreactors, and ultra-low attachment plates, that allow cells to aggregate (Tatullo et al., 2020).

In vivo models and the problem with quiescence

The most common *in vivo* model for assessing cancer therapy is the ectopic transplantation of established cell lines in immunodeficient mice (Gómez-Cuadrado et al., 2017). This model leads to the rapid proliferation of cancer cells and poorly recapitulates cancer cell quiescence (Gómez-Cuadrado et al., 2017). This is applicable to most *in vivo* models of cancer drug evaluation. Micrometastasis is avascular and serves as a suitable model for cancer cell quiescence; however, it is more difficult to model *in vivo* (Gómez-Cuadrado et al., 2017). The need for *in vivo* models of quiescent cancer cells is substantial (Phan and Croucher, 2020).

Hollow fiber assay

The hollow fiber assay was originally developed by Hollingshead et al. (1995) as an economic alternative to the cumbersome xenograft model, which was used for the preliminary assessment of chemotherapy *in vivo* (Hollingshead et al., 1995). Using the hollow fiber assay, fewer animals can be used for a shorter period of time to achieve comparable data regarding a compound's antineoplastic capabilities. This assay has been used by the National Cancer Institute (NCI) to assess chemotherapy in an initial triage to decide which compounds should be evaluated in more advanced *in vivo* models, such as the xenograft (Decker et al., 2004).

In the hollow fiber assay, cancer cells are grown in retrievable packages (macrocapsules) and implanted in animals that are treated with the chemotherapy of choice. Cell viability can then be quantified *ex vivo* using colorimetric tetrazolium-based assays (Hollingshead et al., 1995). The macrocapsules were originally filled with 1–10 10^6 cells/ml cell suspensions and incubated for 24 h prior to implantation in animals. Then, an additional 24-hour incubation was conducted in animals prior to the treatment. This resulted in a sparse-cell macrocapsule with a proliferating cell population (Hollingshead et al., 1995).

Quiescent cancer cells and their response to drug treatment

Quiescent cancer cells have increased resistance to chemotherapy, and cells residing in an otherwise extinguished tumor can potentially lead to relapse and metastasis. Therapies targeted toward specific vulnerabilities in quiescent cancer cells are therefore imperative for decreased relapse and metastasis in patients with hypoxic tumors (Wenzel et al., 2014).

Several drug screenings have been performed for quiescent cancer cells, revealing mitochondrial OXPHOS to be a unique metabolic dependency in quiescent cancer cells (Wenzel et al., 2014; Zhang et al., 2016). The identification of mitochondrial inhibitors as possible cancer treatments has opened the door for drug repurposing. Drug repurposing is a strategy for identifying new treatments by analyzing compounds used in other indications. It involves less risk, since the compounds, if registered, have already been deemed safe to use and the side effects are known (Pushpakom et al., 2019).

Nitazoxanide

In a pharmacological screening performed on MCTS in 2015, compounds that selectively kill quiescent cancer cells were identified – all of which affect mitochondrial metabolism. Niclosamide and nitazoxanide were two of the compounds with the highest efficacy, both of which are antiparasitic compounds suitable for drug repurposing. Nitazoxanide was validated in a xenograft study in mice in combination with irinotecan. This combination decreased tumor size and increased survival (Senkowski et al., 2015).

Nitazoxanide is a Food and Drug Administration (FDA)-approved antimicrobial for oral administration; it was synthesized in the 1970s. Nitazoxanide has broad applications for different types of infections, such as parasitic worms, protozoa, and a wide range of viral infections. Apart from influenza, hepatitis C, and B, nitazoxanide has also been considered a treatment option for COVID-19 due to the *in vitro* inhibition of SARS-CoV 2 (Mahmoud et al., 2020). Tizoxanide, nitazoxanide's active circulating metabolite, has shown activity on a wide range of bacteria, such as *Mycobacterium tuberculosis* and *Clostridium difficile* (Rossignol, 2014). Due to its wide applications, nitazoxanide has been administered to over 75 million people and has caused only mild side effects (Rossignol, 2014).

Since nitazoxanide was primarily developed for the treatment of gastrointestinal infections, it is well tolerated at high doses and has a short half-life in plasma. Nitazoxanide is metabolized by plasma esterases into tizoxanide and excreted in urine and feces, with or without the glucuronic acid added by the liver (Broekhuysen et al., 2000).

Observations of nitazoxanide's efficacy in MCTS *in vitro*

As previously shown in the screening performed by Senkowski et al. (Senkowski et al., 2015), nitazoxanide is selectively toxic to quiescent cancer cells grown in MCTS. The context-dependent vulnerability to nitazoxanide is evident when the same cell line (HCT116-GFP) is cultured as 2D and 3D and treated with nitazoxanide (figure x).

When monolayer cells are seeded 24 h prior to treatment and seven-day quiescent MCTS are incubated with nitazoxanide for 72 h, the graphs separate. Nitazoxanide is clearly 3D selective.

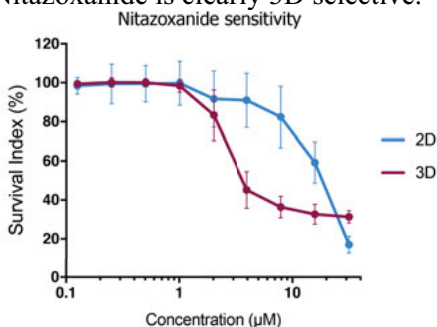


Figure 4. HCT116-GFP are more sensitive to nitazoxanide when grown in a 3D culture (MCTS) compared to 2D culture (monolayer). Dose-response curves for drug treatment: nitazoxanide 0.125–32 µM. Mean and SD, three replicates, n = 24.

When HCT116-GFP MCTS are treated with nitazoxanide and conventional chemotherapy (i.e., irinotecan), GFP detection in IncuCyte reveals that nitazoxanide kills the quiescent cancer cells in the center of MCTS, whereas irinotecan kills the proliferating cells in the MCTS' periphery.

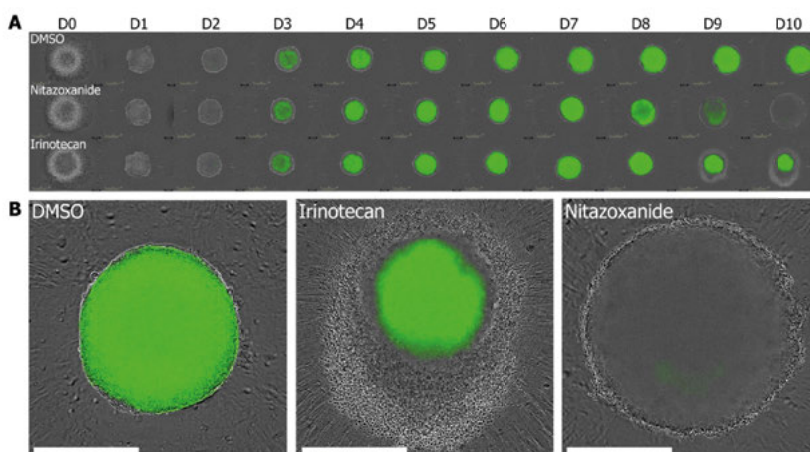


Figure 5. Nitazoxanide kills quiescent MCTS from the inside. Spheroids scanned in the IncuCyte S3 Live-Cell Analysis System (Essen Bioscience) at day 0–10 treated with 8 µM nitazoxanide and 16 µM irinotecan. Compounds were added on Day 7. Two technical replicates

for each treatment and concentration. Lower panel: zoomed-in images of the dying spheroids on Day 10. Spheroid diameter: 620–670 μm on Day 7; the scale bar is 400 μm .

Irinotecan is specifically toxic to monolayer cultured cells, whereas spheroids remain unaffected unless very high concentrations (32 μM) of irinotecan are reached. A clonogenic assay performed on 72-hour treated MCTS, treated on Day 7, revealed the specific toxicity of nitazoxanide in MCTS (3D) compared with monolayer cultured cells (2D) at low concentrations (3 μM).

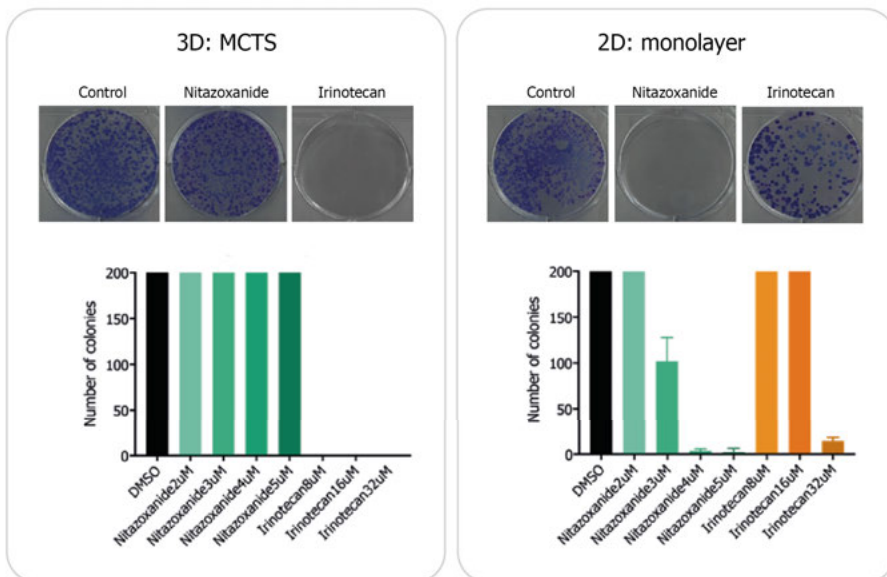


Figure 6. Nitazoxanide effectively decreases clonogenicity in MCTS (3D) while leaving monolayer (2D) cells unaffected. Images of wells: nitazoxanide (5 μM), irinotecan (16 μM).

The mitochondrial membrane potential was disrupted by high concentrations of nitazoxanide in HCT116 cells grown as monolayers.

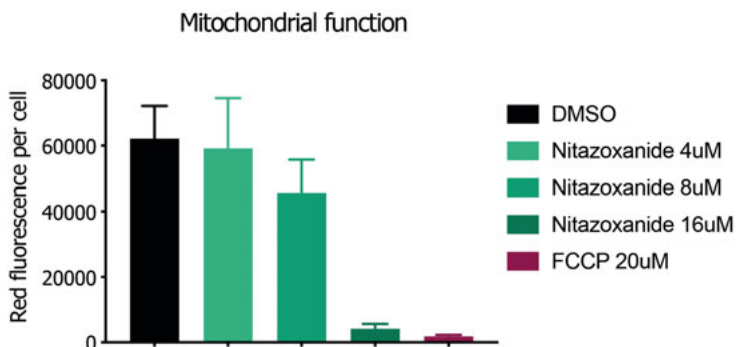


Figure 7. JC-1 assay. Nitazoxanide decreased the mitochondrial membrane potential in the HCT116 monolayer cell culture. FCCP is an uncoupler and positive control.

Culture conditions determine the drug response

Culturing cells in a 3D culture, as done for MCTS, increases cellular density, causing diffusion limitations of nutrients and oxygen. The result is a hypoxic and nutrient-deprived microenvironment with a buildup of H^+ as a result of the anaerobic metabolism. This leads to a decrease in pH. In this microenvironment, the cells become quiescent and dependent on oxidative phosphorylation, as we observed with the increased sensitivity to nitazoxanide in HCT116-GFP cultured in 3D/MCTS compared with a 2D/monolayer cell culture.

The sensitivity in cancer cells to nitazoxanide can also be increased by altering the cell culture conditions by simply conditioning the cell culture media (Senkowski et al., 2016). When HCT116 cells are grown as monolayers 2D/monolayer and 3D/MCTS and treated with nitazoxanide and irinotecan, respectively, in five different types of media, it is obvious that irinotecan treatment is close to unaffected by the different types of media constitution. However, nitazoxanide treatment is potentiated by both a decrease in glucose and pH; pH is the determining factor by far, but glucose can also affect nitazoxanide sensitivity.

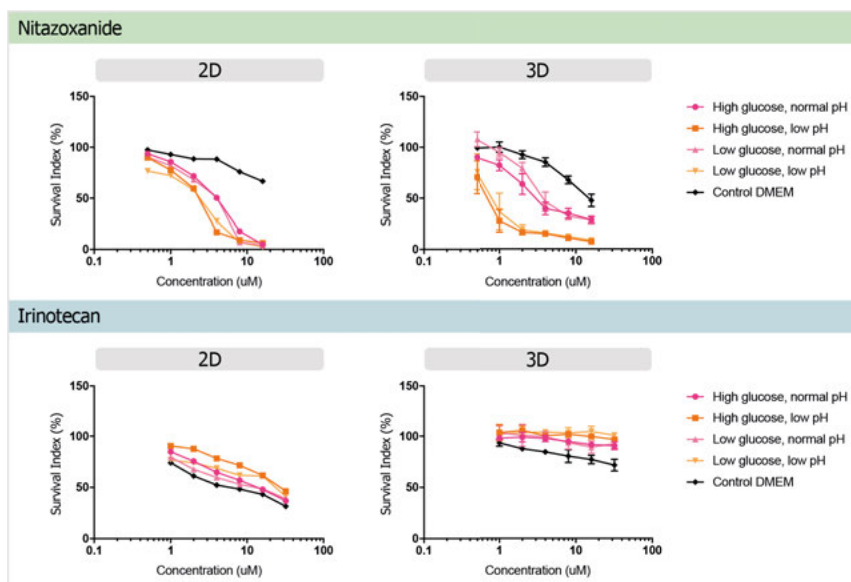


Figure 8. Nitazoxanide's effect on HCT116GFP MCTS (3D) is potentiated by acidic pH. Normal pH: 7.4, acidic pH: ~6.8. N = 3 in each of the three independent replicates. Mean and standard error of the mean (SEM). High glucose: ~20 mmol/l. Low glucose: ~5 mmol/l.

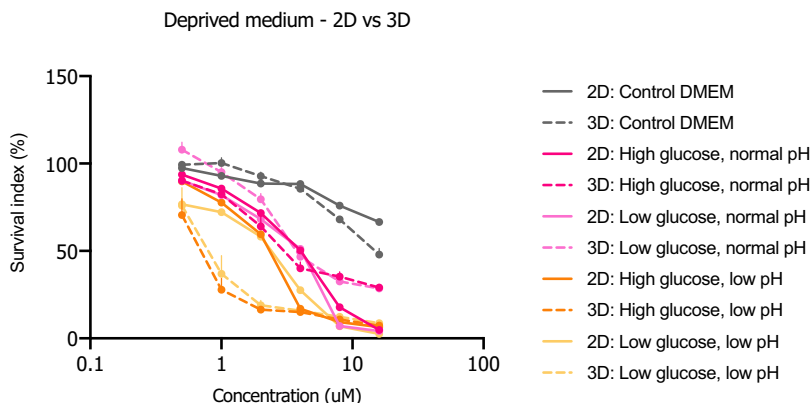


Figure 9. The same data as in Figure 8 for nitazoxanide-treated monolayer cells (2D) and MCTS (3D). The microenvironment seems to be a stronger determinant of nitazoxanide response compared with the cell model (2D vs. 3D) since the same color graphs (same medium constitution) group together in the control medium (dulbecco's modified eagle medium (DMEM)) and normal pH (independent of glucose concentration). In the low pH (~6.8) groups, MCTS (3D) has stronger efficacy compared to 2D.

Sorafenib and regorafenib in advanced stages of HCC

In the advanced stages of HCC, only systemic treatment options are viable. Sorafenib is a multikinase inhibitor. It is the first systemic treatment that prolongs survival in patients with advanced HCC (Yang et al., 2019). Sorafenib prolongs radiological progression and survival by almost three months (Llovet et al., 2008). In previously sorafenib-treated HCC and secondary HCC (primarily colorectal metastasis), regorafenib is used, which is structurally similar to sorafenib but causes more side effects (Yang et al., 2019).

Although clinically effective, regorafenib is not a cost-effective alternative to sorafenib as a second-line therapeutic option for HCC (Juengpanich et al., 2020). The antiangiogenic effects of sorafenib and regorafenib lead to vasculature atrophy and, therefore, insufficient blood supply and hypoxia. Hypoxia-Inducible Factor 1 α (HIF1 α) is upregulated in hypoxia and is considered to be associated with a poor prognosis through immunosuppression, angiogenesis, and metastasis. Hypoxia and HIF1 α upregulation is also associated with resistance to cell cycle active chemotherapy, such as regorafenib (Juengpanich et al., 2020; Kung-Chun Chiu et al., 2019).

Regorafenib has been described as a direct uncoupler of oxidative

phosphorylation and disruptor of mitochondrial membrane potential in primary hepatocytes (Weng et al., 2015)

Aim

The overall aim of this thesis was to develop new 3D models of quiescent cancer cells for the preclinical evaluation of new and current cancer drugs, with an emphasis on the inhibitors of mitochondrial OXPHOS in hepatocellular and colorectal carcinoma.

Paper I

Sorafenib and nitazoxanide disrupt mitochondrial function and inhibit regrowth capacity in three-dimensional models of hepatocellular and colorectal carcinoma

To investigate whether the off-target effect on mitochondrial OXPHOS caused by sorafenib could be connected to the efficacy against quiescent cancer cells in 3D models.

Paper II

The hollow fiber assay for modeling quiescent cancer cells in vitro and in vivo

To develop a quiescent hollow fiber assay to be used *in vivo* for the assessment of compounds targeting quiescent cancer cells.

Methods

Cell culture

Cell lines were subcultivated twice a week in cell culture flasks and incubated at 37 °C in 5% CO₂. HCT116-GFP (Anticancer) HCT116 HRP EGFP (containing EGFP (enhanced GFP)-cDNA with a hypoxia-responsive promoter (HRP)) were cultured in McCoy's 5A medium (M8403, Sigma-Aldrich). Hepatocellular carcinoma cell lines HUH7 and HepG2-GFP were cultured in DMEM (D6546, Sigma-Aldrich). All cell culture medium was supplemented with 10% HI FBS (F9665, Sigma-Aldrich) 2 mM glutamine (G7513, Sigma-Aldrich) and Penicillin (100U/ml)/Streptomycin (100 µg/ml) (P4333, Sigma-Aldrich). Accumax was used to detach the cells for subcultivation. All cell lines were checked for mycoplasma infection and sent to Eurofins Genomics (Ebersberg, Germany) for cell line authentication using DNA and short tandem repeat profiles.

Multicellular tumor spheroid culture and growth

Cells were seeded (5000 cells/50µl/well) into 384-well spheroid microplates (3830, Corning) and centrifuged at 200 g for 5 minutes. Spheroids were formed over seven days without interference or medium change at 37 °C in 5% CO₂. A Breathe-Easy sealing membrane (Z380059, Sigma-Aldrich) was used to minimize evaporation and prevent contamination and sample spillage.

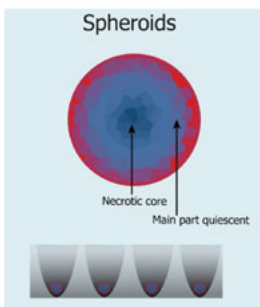


Figure 10: Schematic of the spheroid formation in a 364-well plate.

Monolayer cell seeding

HCT116-GFP cells were seeded from suspension (2500 cells/well, 50 μ l/well) using Biomek 4000 (Beckman Coulter) into Nunc™ 384-well clear Polystyrene plates (ref. 164688, Thermo Fisher Scientific).

Patient cell preparation

Colorectal carcinoma samples were collected in sterile transport media, minced, and enzymatically treated to obtain a cell suspension containing single cells and small aggregates. Successful isolation resulted in a cell suspension with a tumor cell count and viability greater than 70%, respectively. The cells were then cryopreserved in freezing media (HI-FBS containing 10% DMSO) and placed in a -150 °C freezer for long-term storage.

Tumoroid culture

Patient cells (0.5×10^6 cells/ml) were suspended in ice-cold Cultrex Basement membrane extract (BME) gel and seeded in 20 μ l droplets in 6-well plates at a density of 10 droplets per well. The gel droplets were cured for 30 min at 37 °C in 5% CO₂ before the addition of 3 ml per well of Advanced DMEM/F-12 medium supplemented with 10 ml B-27 (50x), 5 ml N1 (100x), 10 μ g basic fibroblast growth factor, 50 μ l epidermal growth factor (EGF), 10 mM HEPES, Penicillin/Streptomycin, 81.6 mg N-Acetyl-L-Cystein, 217.2 mg Ala-Gin, and 10 μ M Rock II.

Tumoroid droplets were grown at 37 °C in 5% CO₂ for 21 days, with medium change every 3–4 days. After 21 days, 2 ml/well of medium was removed, and the plates were placed at 4 °C for 30 min to loosen up the gel. All gel droplets were moved to a 50 ml Falcon tube and centrifuged at 200 g for 10 min. The tumoroid cell pellet was washed with PBS 2–3 times with centrifugation at 200 g for 10 min to remove the gel. The tumoroids were split into two separate tubes; one was subjected to immunohistochemistry (IHC) staining (see Immunohistochemistry), and the other was treated with Accumax to separate the structures further before seeding the tumoroids in 384-well plates in the same medium as above at a density of 5000 cells/45 μ l/well and incubating for 24 h at 37 °C in 5% CO₂ prior to treatment with the drugs added using an Echo 550 Liquid handler. After 3 days, the viability of the tumoroids was analyzed using CellTiterGlo or FMCA.

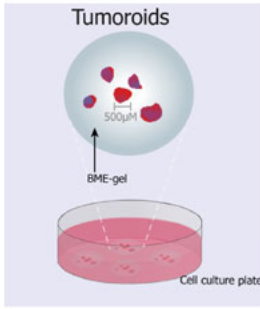


Figure 11: Schematic of the tumoroid formation in the droplets of the BME gel cultures in a 6-well plate

Preparation and cell culture inside hollow fiber macrocapsules

Single-cell suspensions of cancer cell lines were injected using a syringe with a 0,9 mm needle into sterile polyvinylidene fluoridene (PVDF) hollow fiber implant membranes with a 1-mm diameter (KrosFlo, MWKO 500 kD, VWR) and heat-sealed using needle holders to create 2-cm macrocapsules. The macrocapsules were thereafter placed in the complete medium at 37°C with 5% CO₂. When cultured in an unconditioned/high glucose medium, for growth, the macrocapsules were cultured in tissue culture flasks. To create conditioned media/nutrient-deprived conditions, macrocapsules were grown in 6- or 12-well plates. Medium change was performed by removing the medium and exchanging it with fresh medium by pouring (in flasks) or pipetting (plates). For BME-gel experiments, the cells were mixed with BME-gel before filling the hollow fibers with the cell suspension.

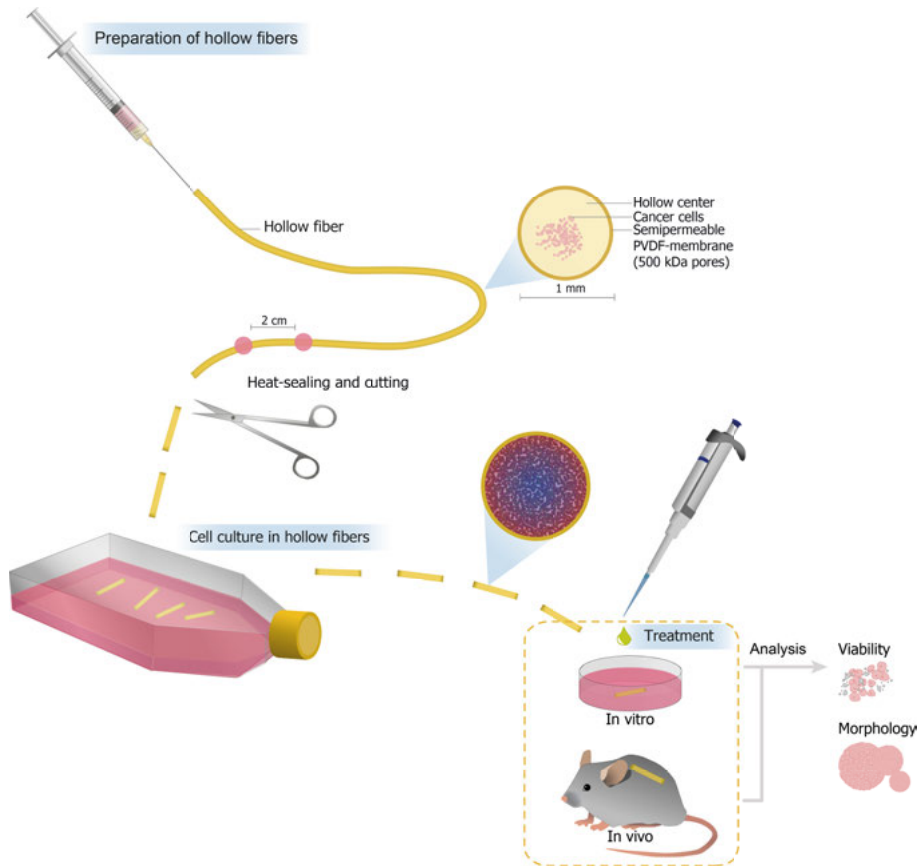


Figure 12. The hollow fiber macrocapsule method for *in vitro* and *in vivo* drug efficacy applications in cancer research. Preparation, cell culture, drug treatment *in vivo* and *in vitro* and analysis.

Galactose experiments

DMEM (11966-025, Invitrogen) free of glucose was supplemented with 10 mM galactose (G5388, Sigma-Aldrich), 2 mM glutamine (G7513, Sigma Aldrich) plus 4 mM before to supplementation to generate a final concentration of 6 mM), 10% HI FBS (F9665, Sigma-Aldrich), 1 mM sodium pyruvate (P5280, Sigma-Aldrich), and Penicillin (100 U/ml) and Streptomycin (100 µg/ml) (P4333, Sigma-Aldrich). High-glucose media. DMEM (11995-065, Invitrogen) containing 25 mM glucose and 1 mM sodium pyruvate. Supplemented with 10% HI FBS (F9665, Sigma-Aldrich) and Penicillin (100 U/ml) and Streptomycin (100 µg/ml) (P4333, Sigma Aldrich). HCT116-GFP and Huh-7 were grown in galactose-containing media and high glucose media respectively. The cells were kept in 5% CO₂ at 37 °C and were cultured for at least six passages before experiments were performed.

Drug treatment

Acoustic drug dispensing

Compounds were added to cells in monolayer and MCTS by acoustic dispensing using Echo 550 Liquid Handler (Labcyte Incorporated). Spheroids were cultured for seven days before treatment while monolayer cells were treated 24 hours after seeding. All compounds were dissolved and diluted in dimethyl-sulfoxide (DMSO).

Manual drug dispensing

The hollow fiber macrocapsules were treated in 6- or 12-well plates in which Nitazoxanide was prepared at the correct concentrations in the cell culture medium. Cells were exposed to the drug treatment for 72 hours at 37 °C in 5% CO₂.

Live cell imaging

IncuCyte S3 Live-Cell Analysis System (Essen Bioscience) was used for all imaging. For spheroid imaging the spheroid module Basic Analyzer was used and either imaged using green or red channel depending on fluorescence wavelength. Hollow fiber macrocapsules were scanned in the green channel and phase contrast. Hollow fiber macrocapsules were scanned in 6- or 12-well plates in their cell culture medium either on-demand or over a sustained period to detect changes in green fluorescence levels. Harvested 3D-structures and cell masses were scanned in 96-well plates. Whole-well scanning settings were used in most experiments. Software version 2017A.

ATP-assay

CellTiterGlo 3D (G9682, Promega) was implemented according to the manufacturer's recommendations, and luminescence was measured using a microplate reader (FLUOstar Omega, BMG LabTech). CellTiterGlo on MCTS was analyzed in 384-well ultra low attachment plates and on hollow fiber macrocapsules in flat 96-well plates. All plates used for the CellTiterGlo assay were black with a clear bottom to prevent luminescence bleeding between wells.

The fluorometric cytotoxicity assay

The fluorometric cytotoxicity assay (FMCA) was conducted in 384-well plates 72 hours post-treatment. FMCA is based on the conversion of FDA into fluorescein by cells with intact plasma membranes (Lindhagen et al., 2008). The plates were centrifuged for 1 minute at 200rpm, the media removed and the cells washed with PBS twice. Q2-buffer consisting of 125mM NaCl, 5.9 mM KCl, 0.5 mM MgCl₂, 0.5 mM CaCl₂ and 25 mM Hepes was added as well as fluorescein diacetate (FDA) (0.5 mM/ml). The cells were incubated with the FDA-solution for 50 minutes at 37°C and the hydrolysis of FDA measured as fluorescence using CLARIOstar Monochromator Platereader (BMG Labtech). Survival index (SI%) is the fraction of the surviving cells per experimental well relative to the average surviving cells in the unexposed control wells.

MTT assay

Macrocapsules were stained using 3-[4,5-dimethylthiazol-2-yl]-2,5-diphenyltetrazolium bromide (MTT solution) for 4 h at 37°C. The macrocapsules were washed in PBS containing 2.5% protamine sulfate overnight at 4 °C and then cut in half and dried overnight. The formazan was extracted by incubating the capsules in DMSO for 4 h at room temperature. Absorbance was read at 570 nm using a microplate reader (FLUOstar Omega, BMG LabTech).

Immunohistochemistry

Pimonidazole is a hypoxia marker suitable for hypoxia detection in 3D cultures *in vitro*. However, pimonidazole staining of *in vivo* samples needs to be conducted several hours prior to surgical resection, making it a less useful marker compared to staining, which can be performed on an already resected sample (Vaupel et al., 2004). KI-67, a marker of proliferation, can be used in prepared samples. Where proliferation is high, oxygen levels and nutrient supply have most likely been rich.

Clonogenic assay

Spheroid preparation for clonogenic assay

HCT116-GFP spheroids (see Spheroid culture) were treated using an Echo Liquid Handler (Labcyte Inc.) on Day 7 and incubated with the drugs for 24, 48, and 72 h at 37°C in 5% CO₂. The spheroids were dispersed using Accumax (50 µl/well, 30 min, 37°C in 5%) and meticulous pipetting until a single-cell solution was achieved. The plate was centrifuged for 5 min at 200 rpm. Accumax was aspirated using an Elx405 Select Deep Well Washer

(BioTek), and 50 μ l new medium was added per well. From each well, 10 μ l was transferred to the well of a 6-well plate (140685, Thermo Scientific) containing 3 ml of medium.

Hollow fiber macrocapsule preparation for clonogenic assay

Cells were harvested from macrocapsules by cutting the sealed edges of the macrocapsules and manually flushing out the cells using accumax. After accumax incubation at 37°C for 30 minutes, the single-cell suspension was counted and an equal number of cells per sample was transferred into 6-well plates.

Staining of colonies

The colonies were allowed to grow for 10 days at 37°C in 5% CO₂ before they were briefly washed with PBS (D8537, Sigma Aldrich), fixated with methanol (A456-1, Fisher Scientific), and stained for 30 min at room temperature with 5% Giemsa (HX263489, Merck) solution in PBS. The Giemsa solution was washed off with water, the colonies were manually counted, and the plates were scanned using a Canon Image Runner Advance C5535i printer (Canon) at a resolution of 600×600 dpi.

JC-1 2D

2500 cells/well in 50 μ l medium were seeded into the 384-well black plates with clear bottom (Nunc 142761) for 48 hours before drug addition (see Acoustic dispensing) using Elx405 Select Deep Well Washer (BioTek) and cultured for 48 hours before aspirating medium and adding staining solution (2,5mg/ml JC-1 and 8,95mg/ml Hoechst 33342 in PBS). The staining solution was incubated with the cells for 20 minutes before washing the cells three times with PBS. The plate was then analysed using Arrayscan VTI reader (Thermo Fisher scientific/Cellomics), confocal module. The 20x objective, blue and red channel was used to acquire images of the Hoechst and JC-1 staining. The mitochondrial polarization was analysed as the mean intensity from detected spots (mitochondria) within objects (cells) using BioApplication Spot Detector (Cellomics Inc.). At least 1,000 cells per well were analysed and at least 4 wells per condition were measured.

JC-1 3D

After aspiration of the medium, spheroids (see Spheroid culture above) were incubated with 35 μ l 3.58 μ g/ml JC-1(T4069, Sigma) in PBS for 30 minutes at 37°C in 5% CO₂ and washed with 50 μ l PBS/well twice before 50 μ l of medium was added to each well. The spheroids were treated with drugs using

an Echo 550 Liquid Handler. The plate was centrifuged at 200 g for 5 min, and the spheroids were incubated with the drugs for 2 h before they were scanned in the IncuCyte S3 Live-Cell Analysis System (Essen Bioscience). The spheroid module Basic Analyzer, 10x, was used to plot the red image mean uncorrected. Fluorescence was calculated as the percentage of control in MS Excel for all individual wells. HCT116: N = 12 within three replicates. Huh-7: N = 16 within four replicates.

CellTiterGlo 3D

The viability of the macrocapsules was analyzed using CellTiterGlo 3D (G9682, Promega) according to the manufacturer's recommendations, and luminescence was measured using a microplate reader (FLUOstar Omega, BMG LabTech).

Library of Integrated Network-Based Cellular Signatures-analysis

Clue touchstone (Broad institute) version 1.1.1.2. L1000 is a Library of Integrated NetworkbasedCellular Signatures (LINCS) where transcriptomic profiles of pharmacologic screening data across nine cell lines are generated and matched to perturbations with similar transcriptomic profiles. Touchstone is a tool in which ~ 3000 annotated compounds with known activities and targets are matched to the compound-induced transcriptomic profile of choice. Sorafenib was used as a seed compound for the similarity search.

Statistics

Raw data were analyzed in MS Excel and GraphPad Prism (version 8.1.1 for macOS). The concentration–response graphs obtained from the viability analysis in paper I were analyzed using half-maximal inhibitory concentration (IC50) calculations in GraphPad Prism. Raw data from the mitochondrial membrane potential assay and the colony regrowth potential assay in paper I were analyzed using one-way analysis of variance (ANOVA), followed by Dunnett's multiple comparisons. The combined effect of the viability and mitochondrial membrane potential was analyzed using the MacSynergy tool.

Results and Discussion

Paper I

Sorafenib and nitazoxanide disrupt mitochondrial function and inhibit regrowth capacity in three-dimensional models of hepatocellular and colorectal carcinoma

Frida Ek, Kristin Blom, Tove Selvin, Jakob Rudolfelt, Claes Andersson, Wojciech Senkowski, Christian Brechot, Peter Nygren, Rolf Larsson, Malin Jarvius, Mårten Fryknäs
Scientific Reports 2022, <https://doi.org/10.1038/s41598-022-12519-4>

Results

Sorafenib shares similarities with OXPHOS inhibitors

The tyrosine kinase inhibitors sorafenib and regorafenib have been reported to affect mitochondria (J. Zhang et al., 2017) in two-dimensional cell cultures (Weng et al., 2015; C. Zhang et al., 2017), and the global transcription profile of nine cell lines post sorafenib treatment generated from the LINCS database indicates that sorafenib is more similar to OXPHOS inhibitors compared with other kinase inhibitors.

Sorafenib, regorafenib, and nitazoxanide kill quiescent cancer cells in 3D cell models

Sorafenib, regorafenib, and nitazoxanide efficiently kill quiescent cancer cells in HCT116 (colorectal carcinoma) and HUH7 (hepatocellular carcinoma) MCTS as well as colorectal carcinoma tumoroids. Conventional chemotherapy, such as irinotecan and 5-FU, does not affect cell viability, whereas kinase inhibitors have an intermediate effect on cell viability.

Sorafenib, regorafenib, and nitazoxanide disrupt mitochondrial function in a new 3D assay

To investigate the effect of sorafenib, regorafenib, and nitazoxanide on the mitochondrial membrane potential in our 3D model of quiescent cancer cells, i.e., MCTS, we adjusted the JC-1 assay, which is generally used to stain monolayer cells to measure changes in the mitochondrial membrane potential ($\Delta\psi_m$) for 3D applications; Ψ_m decreased in MCTS when treated with sorafenib, regorafenib, nitazoxanide, and the positive control and mitochondrial uncoupler carbonyl cyanide-p-trifluoromethoxyphenylhydrazone (FCCP). Other kinase inhibitors and irinotecan did not affect ψ_m . This shows mitochondrial function disruption by sorafenib, regorafenib, and nitazoxanide in quiescent cancer cells in 3D models.

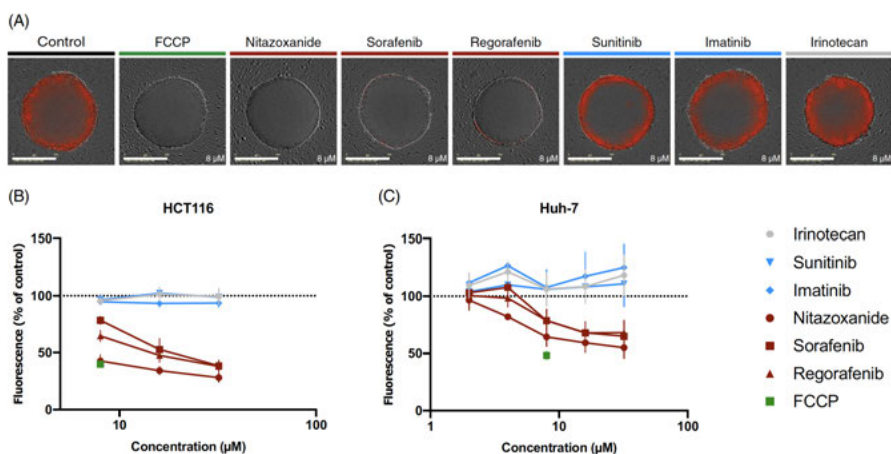


Figure 13. Disruption of mitochondrial function in MCTS. The JC-1 assay was used to visualize alterations in the mitochondrial membrane potential ($\Delta\psi_m$), utilized as a marker for mitochondrial function. (A) Images of HCT116 MCTS treated with seven compounds for 2 h (scale bar = 400 μm). (A–C) Mitochondrial membrane potential ($\Delta\psi_m$) was decreased by nitazoxanide, sorafenib, regorafenib, and the positive control FCCP in Huh-7 MCTS. Huh-7 treated with nitazoxanide, sorafenib, regorafenib, sunitinib, imatinib, and irinotecan: $n = 4$ (quadruplicate wells) for 8–32 μM and $n = 2$ (quadruplicate wells) for 2–4 μM , FCCP: $n = 2$ (quadruplicate wells), CV (controls) = 6.5%–10.6%. HCT116: $n = 3$ (quadruplicate wells), CV (controls) = 7.3%–12.5%. $\Delta\psi_m$ was unaffected by sunitinib, imatinib, and irinotecan compared with the control in both cell lines. (B, C) Graphs depicting $\Delta\psi_m$ as % red fluorescence compared to the control (mean \pm SEM).

Colony regrowth potential is decreased by increased sorafenib and nitazoxanide exposure duration

In exposure duration experiments (24, 48, and 72 h), the colony regrowth potential (clonogenic assay) decreased when the treatment duration of sorafenib and nitazoxanide was increased. The effect of sorafenib on colony

regrowth potential is prominent compared with that of imatinib, which did not have any visible effect.

Sorafenib and nitazoxanide show great promise in combination

The combination of sorafenib and nitazoxanide displayed additive effects on viability, mitochondrial function, and colony regrowth potential. This indicates its potential as a combination therapy to target quiescent cancer cells.

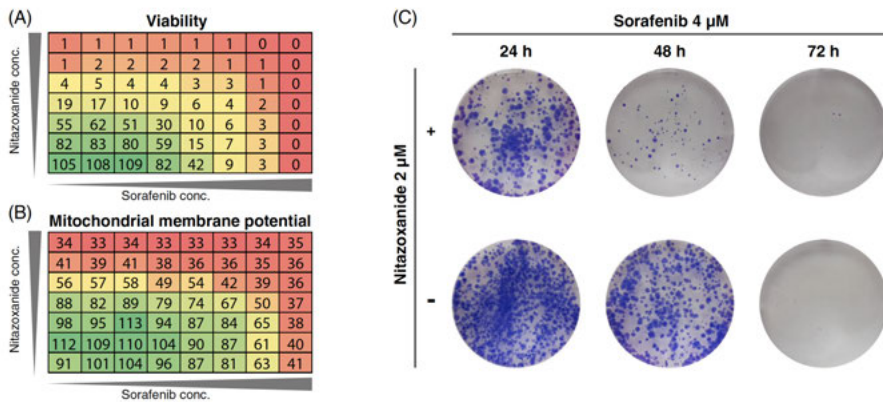


Figure 14. Combining sorafenib and nitazoxanide generates additive effects in HCT116 MCTS. (A, B) MCTS were treated with nitazoxanide (1–32 μ M) and sorafenib (0.5–32 μ M) in a combination matrix for 72 h, resulting in additive effects in both the viability using the ATP assay analyzed using the MacSynergy tool (A, $n = 3$ (quadruplicate wells), survival % of control), and $\Delta\psi_m$ (B, $n = 2$ (quadruplicate wells), fluorescence % of control). (C) MCTS treated with sorafenib (4 μ M) in combination with nitazoxanide (2 μ M) for 48 h and 72 h decreased the colony regrowth potential [$n = 2$ (triplicate wells)].

Discussion

In this paper, we investigated the relationship between the previously reported off-target effect of sorafenib, a tyrosine kinase inhibitor, and regorafenib, which is structurally similar to sorafenib. We also evaluated the specific vulnerability in 3D cultures caused by mitochondrial inhibitors. Compared with other kinase inhibitors that lack this off-target effect on mitochondria, the global transcription profiles induced by sorafenib are more similar to those induced after treatment with inhibitors of mitochondrial OXPHOS.

Sorafenib, regorafenib, and nitazoxanide decreased viability in quiescent cancer cells in MCTS and in therapy-resistant colorectal carcinoma tumoroids. The effect of nitazoxanide has been described previously in MCTS (Senkowski et al., 2015), and the fact that the effect of sorafenib has a similar efficacy in both MCTS and tumoroids shows the potential of sorafenib and regorafenib, especially when the tumoroids are so resistant to all other conventional chemotherapies tested. However, the intermediate response to

other kinase inhibitors is interesting, especially the separation between other kinase inhibitors and sorafenib and regorafenib. One important difference is the replicability of MCTS when immortalized cell lines are used and experiments are performed at a high rate with high numbers of replicates in each experiment. MCTS are also uniform in size and shape, which lowers the variance both within experiments and in between. However, when performing experiments on tumoroids, the materials are patient-derived biopsies or surgical tumor resections, which means that the clinical relevance and the heterogeneity of the sample are higher, causing higher variance. The tumoroid dose-response experiment was performed once, with duplicate wells being used in all treatments except for nitazoxanide, which was measured in quadruplicate wells. The low number of replicates and high variance resulted in IC50 calculations with high levels of uncertainty for all treatments, and they were not applicable for the compounds for which the graph was more of a flat line compared with a dose response curve. This was due to the high resistance of the tumoroids. When individual treatment doses were analyzed using one-way ANOVA and Dunett's multiple comparison test, sorafenib and nitazoxanide 10 μ M, as well as regorafenib 30 μ M and dasatinib, crizotinib, and sunitinib 90 μ M, had significantly lower viability compared to untreated tumoroids.

Even though tumoroids would be of the highest clinical relevance and, therefore, interest for such a study, it is much more difficult, cumbersome, time-consuming, and expensive to work with tumoroids. Thankfully, MCTS is a suitable model for our cells of interest: quiescent cancer cells. Therefore, MCTS were used in the rest of the paper.

The application of the JC-1 assay in a 3D culture and the analysis and visualization conducted in IncuCyte are new approaches that we optimized for this paper. In addition, they were more suitable for measuring mitochondrial function in 3D structures than the original 2D assay that we employed previously. The JC-1 assay is based on the JC-1 monomers, eliciting green fluorescence (529 nm) accumulating inside mitochondrial membranes when the membrane potential is high and then eliciting red fluorescence. When MCTS are treated with mitochondrial inhibitors, the membrane potential decreases, causing red fluorescence to turn green due to the disintegration of JC-1 aggregates into monomers. IncuCyte S3 has two color channels: red and green. Thus, theoretically, JC-1 can be measured both as a green monomer and as a red aggregate. However, the red fluorescence is 590 nm in wavelength, which is more similar to the yellow-orange wavelength. This makes the overlap between green and red fluorescence large, and their separation is difficult when both channels are used. Therefore, only red fluorescence was used for detection in the JC-1 3D assay in IncuCyte.

Loss of mitochondrial membrane potential can, apart from mitochondrial function, also be an indicator of apoptosis, and it is important to notice that sunitinib and imatinib do not affect the mitochondrial membrane potential at

the highest tested concentration—32 μ M for both HCT116 and HUH7—while resulting in 10%–20% viability in HUH7 MCTS. HUH7 has a smaller window for red fluorescence detection compared with HCT116, and it elicits low levels of red fluorescence when left untreated, which we have observed previously when working with hepatocytes.

Another characteristic of HUH7 is that they form strong cell–cell attachments in 3D, which results in difficulties disrupting MCTS to single cell suspension. Single-cell suspension is a requirement in clonogenic assays. Therefore, HCT116 was used in the colony regrowth potential assay. Surprisingly, we found that sorafenib had an even stronger effect on colony regrowth potential compared with nitazoxanide, which corroborates the efficacy of using sorafenib in cancer cells in a 3D cell culture.

Cancer cells become quiescent in metabolically inadequate microenvironments, often as a result of aberrant tumor vasculature in combination with unregulated proliferation. Hypoxia is common in hepatocellular carcinoma and is associated with a poor prognosis (Guo et al., 2020). Transarterial chemoembolization (TACE), the first-line treatment for intermediate-stage HCC, is based on the blockage of the blood supply to the tumor in combination with the local administration of high doses of chemotherapy. Due to the blockage of blood supply, hypoxia is inherent to the treatment (Kotsifa et al., 2022), and the addition of sorafenib orally to the TACE treatment alone has been proven to be well tolerated and to increase overall survival in patients suffering from unresectable HCC (Peng et al., 2022; Ren et al., 2019). Our findings highlight the effect of sorafenib on quiescent cancer cells as one probable cause of the effect of sorafenib on quiescent cancer cells in combination with TACE.

Although sorafenib is considered well tolerated (Ren et al., 2019) and is approved for the treatment of unresectable HCC, advanced renal cell carcinoma, and therapy-resistant differentiated thyroid carcinoma (EMA, 2018a), there are dose-limiting side effects, such as renal toxicity, hypertension, cardiovascular events, hand-foot skin reaction, diarrhea, and fatigue (Y. Li et al., 2015). Regorafenib, a structurally similar analog to sorafenib, has a stronger antiangiogenic effect and a more aggressive, yet similar, side-effect profile. Regorafenib is approved for the treatment of treatment-resistant metastasized colorectal carcinoma, treatment-resistant gastrointestinal stromal tumor, and sorafenib-resistant hepatocellular carcinoma (EMA, 2018b).

Nitazoxanide and sorafenib have additive effects on quiescent cancer cells *in vitro*, and nitazoxanide has a safer side-effect profile because its indications are microbial infections, not cancer treatment. Nitazoxanide can reach plasma levels >6 μ M after a single oral dose of 500 mg (Broekhuysen et al., 2000), and it has been administered to over 75 million people with gastrointestinal infections without major drug-related safety issues (Rossignol, 2014, p.). Nitazoxanide is therefore a promising candidate for combination treatment

with sorafenib for HCC. Regorafenib can also be considered for combination therapy with nitazoxanide, given its structural and phenotypical similarities to sorafenib.

Conclusions from Paper I

We show that quiescent cancer cells have a specific sensitivity to nitazoxanide and that sorafenib and regorafenib share this property. This separates them from other multikinase inhibitors and cell-cycle active chemotherapy. The sensitivity of quiescent cancer cells to nitazoxanide, sorafenib, and regorafenib correlates with the disruption of the mitochondrial membrane potential ($\Delta\psi_m$) in quiescent cancer cells in 3D cultures. Nitazoxanide and sorafenib, in combination, cause an additive decrease in viability, mitochondrial function disruption, and colony regrowth capacity, which might have clinical applications.

Paper II

The hollow fiber assay for modeling quiescent cancer cells *in vitro* and *in vivo*

Frida Ek, Tove Selvin, Mårten Fryknäs

Unpublished manuscript

Results

Large 3D structures need space and time to develop

To evaluate the requirements for forming 3D structures in hollow fiber macrocapsules, different culture conditions were evaluated. The colorectal carcinoma cell line HCT116-GFP was grown in hollow fiber macrocapsules for 7 or 14 days with either high or low medium accessibility (tissue culture flasks and 6-well plates). GFP intensity was visualized using the InCuCyte S3 Live-Cell Analysis System as a proxy for cell viability (Senkowski et al., 2015). The 3D structures were visualized through PVDF fiber in 6- and 12-well plates, and they were harvested in 96-well plates using the “whole well” function in InCuCyte. Between days 7 and 14, the 3D structures grew larger and displayed visually higher GFP expression; in addition, the glucose levels in the medium decreased.

Hypoxia and quiescence are enriched in hollow fiber macrocapsules over time

Increased hypoxia over time was visualized in MCTS and hollow fiber macrocapsules using the hypoxia reporter cell line HCT116 HRP EGFP. This proves the presence of hypoxia in the quiescent hollow fiber assay. A hypoxic microenvironment is an important driver of cellular quiescence (Butturini et al., 2019). The achievement of a quiescent state was corroborated by a cell cycle analysis performed on Day 10 compared to Day 0, indicative of the G0/G1 arrest.

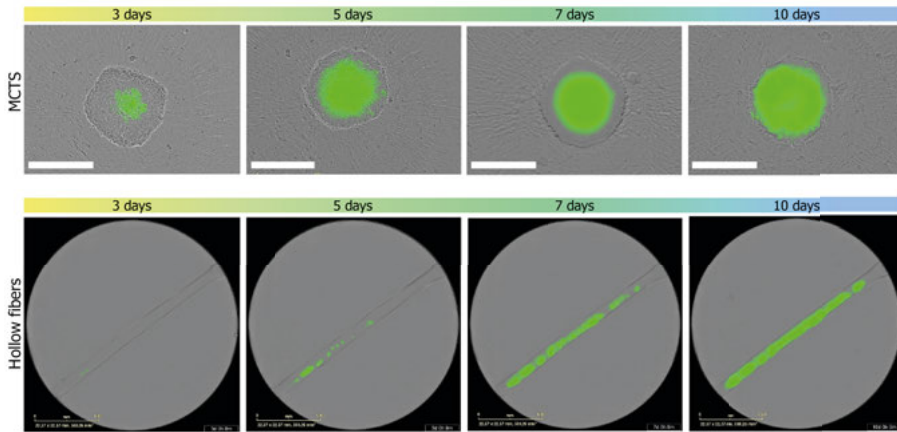


Figure 15. HCT116 HRP EGFP with hypoxia-induced GFP expression grown as MCTS and hollow fiber macrocapsules and visualized on Day 3, 5, 7, and 10. Hypoxia increased over time in both MCTS and hollow fiber macrocapsules.

Quiescent hollow fiber macrocapsules are sensitized to the OXPHOS inhibitor nitazoxanide

Hollow fiber macrocapsules filled with HCT116-GFP were grown in a fresh cell culture medium with approximately 15 mmol/l glucose or a depleted cell culture medium with approximately 6 mmol/l glucose. They were treated with nitazoxanide after 10 days of growth and analyzed using an MTT assay. The depletion of the medium forced the cells into a quiescent state, similar to what was observed in the MCTS model (Senkowski et al., 2015), which sensitized the cells to nitazoxanide.

Quiescence can be achieved by contact inhibition at a high cell density (Nik Nabil et al., 2021). Therefore, the cell density was increased from 1.5 M cells/ml to 10 M cells/ml when filling the macrocapsules. However, no differences were found in either cellular yield or nitazoxanide sensitivity in macrocapsules with vastly different cell densities at Day 0. Increased cell density and cell quiescence at the time of treatment cannot be achieved by increasing cell density from the beginning.

Viability assays and BME-gel as means of method development

The original viability assay, MTT, focuses on metabolic activity and is based on tetrazolium dye. It can be easily used on intact macrocapsules. However, the MTT assay is affected by quiescence because the metabolic inactivity of quiescent cells can provide a false negative result, which is perceived as a low

value in the untreated group. When we compared the MTT assay to an ATP assay, the latter was clearly superior.

When culturing HepG2-GFP cells inside hollow fiber macrocapsules, the cell numbers harvested were low, and the cells seemed to adhere to the fiber walls. By adding Basement membrane extract (BME)-gel the viability of HepG2-GFP improved and the 3D structures grew larger. This indicates that cell lines that have trouble growing in hollow fiber macrocapsules can be assisted by the addition of BME-gel.

In vivo studies

Two *in vivo* studies were conducted to assess how viability is affected by implantation under the skin in the flanks of mice. In parallel to the *in vivo* macrocapsules, some were cultured as they normally are *in vitro*. Two types of mice were used in the first study: athymic with partial immune suppression and NOG, which are completely immune-incompetent. The macrocapsules were left in the mice for five days before they were harvested and analyzed using the ATP assay *ex vivo*. In the first study, two macrocapsules stood out from the rest with a very low ATP signal; however, all other macrocapsules from mice had higher ATP levels compared to those cultured *in vitro*—even fibers that were 7 days older (14 days).

In the second study, BME gel was assessed for *in vivo* use. The ATP levels obtained from the macrocapsules grown in mice were higher than those obtained *in vitro* in this case as well. We can conclude that the *in vivo* environment is favorable for cells growing in hollow fiber macrocapsules.

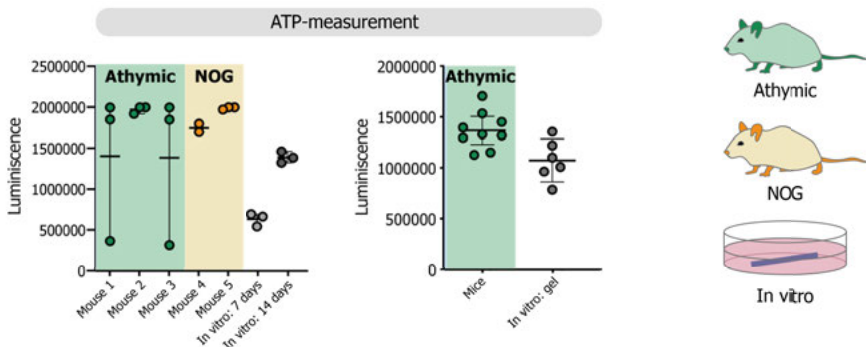


Figure 16. Results from *in vivo* studies: Study 1 (left) and Study 2 (right). HCT116-GFP macrocapsules were implanted in mice after 2 days and harvested after 5 days. In the first study, *in vitro* macrocapsules were grown for 7 and 14 days. In the second study, HCT116-GFP was mixed with BME gel and grown in athymic mice for 5 days and *in vitro* for comparison.

Discussion

Most *in vivo* assays used for the assessment of antineoplastic therapies involve rapid proliferation of cells and uncontrolled tumor growth. To evaluate drugs that specifically target quiescent cancer cells, there is a dearth of assays that model quiescent cancer cells. Therefore, we aimed to develop an assay *in vitro* that could be used *in vivo* for the evaluation of compounds selectively targeting quiescent cancer cells.

Modeling quiescent cancer cells is a difficult task without the presence of an intricate tumor microenvironment (TME) that creates cancer cell quiescence *in vivo* (Nik Nabil et al., 2021). In our quiescent MCTS model, HCT116-GFP is allowed to self-assemble into spheroids in ultra-low attachment plates, and the spheroids become denser each day until a steady state is reached between Day 7 and Day 10. Quiescence is achieved by increased cellular density, causing gradients of oxygen, nutrients, pH, and glucose to form from the periphery toward the center (Karlsson et al., 2019). The hypoxic, nutrient-deprived, and OXPHOS-dependent microenvironment created in the center of dense MCTS is inherent to the model.

A quiescent hollow fiber assay was implemented to transfer the capacities of inherent quiescence in MCTS to PVDF macrocapsules that can be implanted in animals. By doing so, we could bridge the gap between the *in vitro* findings of drugs targeting quiescence and *in vivo* evaluation. By making the method as similar as possible to quiescent MCTS while using PVDF macrocapsules, we posited that HCT116-GFP would self-assemble into large 3D structures with high cellular density and the formation of gradients of nutrients, oxygen, and pH from the periphery toward the center of the macrocapsule. In our quiescent hollow fiber assay, HCT116-GFP self-assembled into large spherical 3D structures that reached a steady state of cell growth after 7–10 days. The diameter of the 3D structures was not larger than that of the MCTS, indicating that the diffusion limitations caused by the cellular density in the 3D structures limited structural growth at approximately 500–600 μM . This steady-state growth and halted proliferation indicate quiescence.

Another characteristic of quiescent MCTS observed in our quiescent hollow fiber macrocapsules was hypoxia. In MCTS hypoxia, we can detect hypoxia by culturing HCT116 HRP EGFP (hypoxia reporter) as MCTS and using live cell imaging to follow the increasing GFP expression through increasing green fluorescence, as we did in this paper. When HCT116 HRP EGFP is cultured inside hollow fiber macrocapsules, we can use live cell imaging in a similar fashion as MCTS and follow the increasing GFP expression as green fluorescence, and thereby hypoxia, over time. However, since spheroids and hollow fibers are not cultured in the same vessel, the levels of hypoxia in the two models cannot be compared. We can only draw conclusions about whether green fluorescence is increasing over time, which

was the case in both assays. The increasing hypoxia indicates increasing quiescence (Nik Nabil et al., 2021) in our hollow fiber macrocapsules.

Cell cycle analysis revealed that the proportion of cells in G0/G1 increased after 10 days inside hollow fiber macrocapsules, and the mitosis peak disappeared, proving the achievement of a quiescent state.

Another characteristic of quiescence is a lack of proliferation, and when MCTS are stained with the proliferation marker KI-67, the proliferating cells in the periphery are stained positive, whereas the quiescent cells in the center of the MCTS are stained negative. We also performed IHC on hollow fiber macrocapsules, but the staining of hollow fiber macrocapsules was more difficult, and the 3D structures were often destroyed either prior to staining or during, which made it difficult to draw conclusions from the stains. One hypothesis is that it was difficult to cut through PVDF fiber, as it was rigid and dense. This could have made it difficult for us to prepare slides without destroying the more fragile 3D structures.

We know that quiescent cells reside in metabolically compromised microenvironments and that they rely on OXPHOS for survival. This causes quiescent cancer cells to have a specific vulnerability to mitochondrial inhibitors, which we can take advantage of when identifying quiescent cancer cells. If their vulnerability to mitochondrial inhibitors is increased, so is the likelihood of them being quiescent. Quiescent MCTS are highly sensitive to the inhibitor of mitochondrial OXPHOS, i.e., nitazoxanide, and when treating hollow fibers with nitazoxanide, we can deduce two things. The HCT116-GFP cells cultured inside our hollow fiber macrocapsules are sensitive to nitazoxanide, and the sensitivity can be increased by aggravating the deficiencies in the microenvironment through further depletion of the cell culture medium. This lowers the pH and glucose levels in the microenvironment, which increases the sensitivity of the cells to nitazoxanide.

Another important characteristic of quiescent cancer cells is their increased therapy resistance to conventional cancer treatment (Nik Nabil et al., 2021). The original plan for this project was to treat quiescent hollow fiber macrocapsules with the IC50 from a monolayer cell culture (2D IC50) to assess their level of resistance to conventional chemotherapy and possible sensitivity to mitochondrial inhibitors. Treatment of quiescent hollow fiber macrocapsules with medications such as irinotecan, doxorubicin, and 5-FU should definitely be investigated in the future.

The results from the HCT116-GFP grown in hollow fiber macrocapsules seem promising, with large quiescent 3D structures growing and surviving *in vitro* and *in vivo*. However, several other cell lines were also tested, which yielded variable results. We attempted culturing HT-29, HepG2-GFP, HUH7, and A549 cells in hollow fiber macrocapsules. HT-29 had poor viability and was ruled out. HepG2, HUH7, and A549 showed high viability. A549 did not form any 3D structures. Although HepG2 and HUH7 formed 3D structures and had high viability, cell harvesting was unstable and provided variable

results, possibly because of the strong cell attachments to the fiber wall. We attempted to encourage cell–cell attachments and cell harvesting by adding BME gel to the HepG2-GFP-cell suspension as well as Accumax to facilitate detachment from the fiber wall. This generated larger 3D structures that were easily harvested from the macrocapsules; however, this made the method even more cumbersome and costly.

The ATP assay, as a viability assay for quiescent hollow fiber macrocapsules, has a higher assay sensitivity compared with the traditionally used MTT assay. The MTT assay protocol includes drying formazan-stained fibers for a minimum of 24 h prior to absorbance measurement. This enables storing fibers from different time points and then analyzing them at the same time and plotting the percentage change from a time point in the timeline of choice. The benefit of this is that the same batch of macrocapsules can be analyzed at the start and finish of the experiments, avoiding variance between batches and affecting the results. The ATP assay (CellTiterGlo) is used in living cells, which means that a macrocapsule from Day 0 cannot be saved until analysis on Day 7, for example. If different ages of hollow fiber macrocapsules are to be compared, they need to be prepared at different time points, which could introduce variance between batches and affect the results.

Implementing an ATP assay for hollow fiber macrocapsules is laborious because the cellular material needs to be emptied from the macrocapsules, which requires steady hands and precision. However, an advantage of this is that, when we empty the macrocapsules, their contents can be analyzed using a microscope and IncuCyte, which enables us to observe the morphology of 3D structures. The ATP assay has been developed to work in flat-well, clear-bottom 96-well plates, which is optimal for both whole-well imaging using IncuCyte and luminescence reading using a plate reader.

Culturing hollow fiber macrocapsules for a week prior to implantation in animals could mimic this change from a high- to low-nutrient microenvironment because it takes around five days for cells inside hollow fiber macrocapsules to attract blood vessels. While absent blood vessels enable a quiescent state, this might make drug delivery difficult, thereby raising the question of exposure in *in vivo* experiments.

Through this project, we have had problems replicating results and large experiments have suffered from inexplicable cell death in hollow fiber macrocapsules. Some of these events might be explained by dysfunctional PVDF-fibers during a period, a tilting incubator shelf for another, and a construction site shaking cells (and optics) to death for a third. Shortcomings in the assay cannot, however, be ruled out entirely. Although our preliminary results seem promising, replicating results is a necessary next step in this project. Through this characterization of the quiescent hollow fiber assay, we learned important lessons for future research.

Conclusions from Paper II

We developed a quiescent hollow fiber assay using HCT116-GFP cells and implemented improved analysis using live cell imaging and ATP analysis. Hypoxia and cancer cell quiescence were enriched in the hollow fiber macrocapsules over time, and the culture conditions affected the nitazoxanide sensitivity. We used BME gel to support cell growth in hollow fiber macrocapsules and implanted macrocapsules in mice. The environment *in vivo* is favorable for cell growth. Through this characterization of the quiescent hollow fiber assay, we learned important lessons for future research.

Concluding remarks and future perspectives

Despite the many efforts in drug development to find efficient cancer therapies, the discrepancy between *in vitro* models and the microenvironment and morphology *in vivo* is believed to be the primary reason why most potential cancer drugs fail in clinical trials. The overall probability of success for cancer drugs in clinical trials is estimated to be 3.4% (Wong et al., 2019). The industry is in dire need of preclinical models with a higher predictive value. Although no *in vitro* model can entirely mimic the complex microenvironment *in vivo*, we can approximate solid tumors by developing new 3D models for drug development and discovery with higher clinical relevance.

This thesis aimed to develop new 3D models of quiescent cancer cells for the preclinical evaluation of new and current cancer drugs, with an emphasis on inhibitors of mitochondrial OXPHOS in HCC and CRC.

We employed current 3D models (MCTS and tumoroids) to evaluate the efficacy of two kinase inhibitors, sorafenib and regorafenib, with reported off-target effects on mitochondria against quiescent cancer cells. A new assay, JC-1, was developed in a 3D cell culture to measure the mitochondrial membrane potential in MCTS, and it was used to conclude that sorafenib and regorafenib decrease mitochondrial function and kill quiescent cancer cells. Sorafenib and nitazoxanide have additive effects on cell viability, mitochondrial function, and colony regrowth potential, thereby making nitazoxanide a candidate for use in combination therapies with sorafenib.

We also embarked on developing a new *in vivo* model for the evaluation of drugs targeting quiescent cancer cells: the quiescent hollow fiber assay. In this assay, cells are cultured inside semipermeable, hollow PVDF fibers and are allowed to self-assemble into 3D aggregates with inherent hypoxia and quiescence. Cells growing in hollow fiber macrocapsules can be supported by BME gel, and the environment is more favorable *in vivo* than *in vitro*.

Other efforts to model quiescent cancer cells *in vivo* often revolve around the concept of metastasis since micrometastases are avascular and quiescent (J. Li et al., 2015; Wells et al., 2013). Among the transplantation models of metastasis, spontaneous models are the most similar to normal xenografts. Ectopic (a histotype different from the transplantation site) or orthopic (same histotype) primary tumors are allowed to spread to secondary sites and therefore model the full metastasis process (Gómez-Cuadrado et al., 2017). In addition, there are spontaneous metastasis models wherein the primary tumor

is resected to allow the assessment of adjuvant therapy for metastasis development. Experimental transplantation models of metastasis include the injection of cancer cells intraperitoneally, intracardially, or into the tail veins of mice (Gómez-Cuadrado et al., 2017).

The results in Paper I (Ek et al., 2022) suggest sorafenib and nitazoxanide as future candidates, in addition to the current treatment with TACE, for targeting quiescent cancer cells in HCC. TACE is performed by injecting drugs into the hepatic artery, supplying the tumor with oxygen, and creating a synthetic embolus by injecting particles that block the blood supply (Yang et al., 2019). HCC tumors have avascular areas with hypoxia, and TACE reinforces this oxygen deprivation. Sorafenib and regorafenib, which are both used in advanced-stage HCC, further aggravate hypoxia by causing an anti-angiogenic effect.

Nitazoxanide, sorafenib, and regorafenib can only be administered orally due to their poor solubility in aqueous media (National Center for Biotechnology Information, 2022a, 2022b; Sood et al., 2021). TACE is often used with high concentrations of chemotherapy administered locally (Kotsifa et al., 2022), and future research should investigate the possibility of local administration of drugs targeting quiescent cancer cells. Efforts have been made to increase the solubility of nitazoxanide (Sood et al., 2021) and to incorporate nitazoxanide in laser-responsive liposomes that release nitazoxanide at the tumor site (Darwish et al., 2018). The increased solubility of nitazoxanide and sorafenib and finding new compounds sharing the same specific toxicity to quiescent cancer cells is something that should be investigated in future research.

TACE is interesting not only from the perspective of the clinical applications of our findings in HCC but also as a possible model of quiescent cancer cells *in vivo*. It is also one of the few procedures in which drugs are injected intratumorally (He et al., 2015), which makes TACE models in mice an interesting candidate for *in vivo* validation of nitazoxanide with improved solubility. Intratumoral injection of regorafenib-loaded polymeric microspheres is an example where attempts have been made to increase the drug effect locally in TACE-treated HCC (Li et al., 2020).

It is evident from our research that the culture conditions determine drug sensitivity and that the sensitivity of cancer cells to nitazoxanide increases in microenvironments with hypoxia, acidic pH, and low glucose levels. These conditions are inherent to 3D cell models but can also push monolayer cell cultures into increased nitazoxanide sensitivity or further aggravate the sensitivity in 3D cultures. The nitazoxanide sensitivity is greatly affected by treating quiescent hollow fibers in new or conditioned (nutrient-deprived) media, even though the 3D structures are of the same age and size. This context-dependent sensitivity is crucial and should be considered in future studies using nitazoxanide and other mitochondrial inhibitors. Conditioned cell culture media and a microenvironment that is hypoxic, acidic, and glucose-deprived will push cancer cells toward OXPHOS dependence and

will therefore increase the sensitivity of cancer cells to mitochondrial inhibitors.

Cancer often finds new ways to adapt to and survive our endless attempts to eradicate cancer cells, and there are countless theories and ideas on what the “magic cure” for cancer could be. Without the cancer characteristic of uncontrolled proliferation, cancer would seldom constitute a problem; therefore, antiproliferative treatment will always be crucial. Quiescent cancer cells are resistant to antiproliferative treatment, which would not constitute a problem unless they re-enter the cell cycle due to metabolic plasticity and regain the capacity to rapidly proliferate when conditions change, causing metastatic and local recurrence. By targeting quiescent cancer cells as a complement to antiproliferative treatment, the idea is to kill quiescent cancer cells before they have the opportunity to become highly proliferative and cause recurrence (Wells et al., 2013).

Through this development and characterization of models of quiescent cancer cells, for preclinical evaluation of new therapeutics, we have outlined potential paths for future research.

Acknowledgements

I would like to express my deepest gratitude to my main supervisor, Mårten Fryknäs, for their enthusiasm, inspiring ideas, invaluable patience, and optimism. I am deeply indebted to my co-supervisors, Malin Jarvius, for their scientific knowledge, creative inspiration, and crucial moral support, and Professor Rolf Larsson, for providing me with the opportunity to work on this research and for sharing your extensive expertise in science. I am grateful to Professor Anders Backlund, Pär Hallberg, Katarina Jonasson Vangen, Gabriella Widerberg, Anna Sjöström, and Professor Mia Wadelius. Thank you for your kindness and support.

I could not have undertaken this journey without Tove Selvin, who worked side by side with me, like a conjoined twin, in the lab. Thank you for staying by my side (literally), cursing, laughing, and color coding in an office with an all-year Christmas spirit. Thank you, Jenny Rubin, for believing in me and hyping me up when I needed it the most. I would also like to extend my sincere thanks to all of my friends and colleagues who supported me and cheered me on over the years.

I am extremely grateful to my family, who endured all ups and downs of this process while always offering encouragement and love. This endeavor would not have been possible without my best friend and love of my life Peter. You have been my Samwise Gamgee during this journey, and even though you could not carry the thesis for me, you carried me.

Most of all, I am grateful to my son, William, who taught me to play, laugh, and love unconditionally. Even the smallest person can change the course of the future, and I am forever grateful.

References

- Birsoy, K., Possemato, R., Lorbeer, F.K., Bayraktar, E.C., Thiru, P., Yucel, B., Wang, T., Chen, W.W., Clish, C.B., Sabatini, D.M., 2014. Metabolic determinants of cancer cell sensitivity to glucose limitation and biguanides. *Nature* 508, 108–112. <https://doi.org/10.1038/nature13110>
- Broekhuysen, J., Stockis, A., Lins, R.L., De Graeve, J., Rossignol, J.F., 2000. Nitazoxanide: pharmacokinetics and metabolism in man. *Int J Clin Pharmacol Ther* 38, 387–394. <https://doi.org/10.5414/cpp38387>
- Butturini, E., Carcereri de Prati, A., Boriero, D., Mariotto, S., 2019. Tumor Dormancy and Interplay with Hypoxic Tumor Microenvironment. *Int J Mol Sci* 20, 4305. <https://doi.org/10.3390/ijms20174305>
- Calderaro, J., Couchy, G., Imbeaud, S., Amaddeo, G., Letouzé, E., Blanc, J.-F., Laurent, C., Hajji, Y., Azoulay, D., Bioulac-Sage, P., Nault, J.-C., Zucman-Rossi, J., 2017. Histological subtypes of hepatocellular carcinoma are related to gene mutations and molecular tumour classification. *J Hepatol* 67, 727–738. <https://doi.org/10.1016/j.jhep.2017.05.014>
- Darwish, W.M., Bayoumi, N.A., El-Kolaly, M.T., 2018. Laser-responsive liposome for selective tumor targeting of nitazoxanide nanoparticles. *Eur J Pharm Sci* 111, 526–533. <https://doi.org/10.1016/j.ejps.2017.10.038>
- Decker, S., Hollingshead, M., Bonomi, C.A., Carter, J.P., Sausville, E.A., 2004. The hollow fibre model in cancer drug screening: the NCI experience. *Eur J Cancer* 40, 821–826. <https://doi.org/10.1016/j.ejca.2003.11.029>
- Ek, F., Blom, K., Selvin, T., Rudolf, J., Andersson, C., Senkowski, W., Brechot, C., Nygren, P., Larsson, R., Jarvius, M., Fryknäs, M., 2022. Sorafenib and nitazoxanide disrupt mitochondrial function and inhibit regrowth capacity in three-dimensional models of hepatocellular and colorectal carcinoma. *Sci Rep* 12, 8943. <https://doi.org/10.1038/s41598-022-12519-4>
- EMA, 2018a. Nexavar [WWW Document]. European Medicines Agency. URL

- <https://www.ema.europa.eu/en/medicines/human/EPAR/nexavar>
(accessed 9.2.22).
- EMA, 2018b. Stivarga [WWW Document]. European Medicines Agency. URL
<https://www.ema.europa.eu/en/medicines/human/EPAR/stivarga>
(accessed 9.2.22).
- Endo, H., Inoue, M., 2019. Dormancy in cancer. *Cancer Sci* 110, 474–480.
<https://doi.org/10.1111/cas.13917>
- Finnberg, N.K., Gokare, P., Lev, A., Grivennikov, S.I., MacFarlane, A.W., Campbell, K.S., Winters, R.M., Kaputa, K., Farma, J.M., Abbas, A.E.-S., Grasso, L., Nicolaidis, N.C., El-Deiry, W.S., 2017. Application of 3D tumoroid systems to define immune and cytotoxic therapeutic responses based on tumoroid and tissue slice culture molecular signatures. *Oncotarget* 8, 66747–66757.
<https://doi.org/10.18632/oncotarget.19965>
- Gómez-Cuadrado, L., Tracey, N., Ma, R., Qian, B., Brunton, V.G., 2017. Mouse models of metastasis: progress and prospects. *Dis Model Mech* 10, 1061–1074. <https://doi.org/10.1242/dmm.030403>
- Guo, Y., Xiao, Z., Yang, L., Gao, Y., Zhu, Q., Hu, L., Huang, D., Xu, Q., 2020. Hypoxia-inducible factors in hepatocellular carcinoma. *Oncol Rep* 43, 3–15. <https://doi.org/10.3892/or.2019.7397>
- Hadfield, G., 1954. The Dormant Cancer Cell. *Br Med J* 2, 607-610.1.
- Hanahan, D., Weinberg, R.A., 2000. The hallmarks of cancer. *Cell* 100, 57–70. [https://doi.org/10.1016/s0092-8674\(00\)81683-9](https://doi.org/10.1016/s0092-8674(00)81683-9)
- He, L., Tian, D.-A., Li, P.-Y., He, X.-X., 2015. Mouse models of liver cancer: Progress and recommendations. *Oncotarget* 6, 23306–23322.
- Hollingshead, M.G., Alley, M.C., Camalier, R.F., Abbott, B.J., Mayo, J.G., Malspeis, L., Grever, M.R., 1995. In vivo cultivation of tumor cells in hollow fibers. *Life Sci* 57, 131–141. [https://doi.org/10.1016/0024-3205\(95\)00254-4](https://doi.org/10.1016/0024-3205(95)00254-4)
- Holmgren, L., O'Reilly, M.S., Folkman, J., 1995. Dormancy of micrometastases: balanced proliferation and apoptosis in the presence of angiogenesis suppression. *Nat Med* 1, 149–153.
<https://doi.org/10.1038/nm0295-149>
- Juengpanich, S., Topatana, W., Lu, C., Staiculescu, D., Li, S., Cao, J., Lin, J., Hu, J., Chen, M., Chen, J., Cai, X., 2020. Role of cellular, molecular and tumor microenvironment in hepatocellular carcinoma: Possible targets and future directions in the regorafenib era. *Int. J. Cancer* 147, 1778–1792. <https://doi.org/10.1002/ijc.32970>
- Karlsson, H., Fryknäs, M., Larsson, R., Nygren, P., 2012a. Loss of cancer drug activity in colon cancer HCT-116 cells during spheroid formation in a new 3-D spheroid cell culture system. *Experimental Cell Research* 318, 1577–1585. <https://doi.org/10.1016/j.yexcr.2012.03.026>
- Karlsson, H., Fryknäs, M., Larsson, R., Nygren, P., 2012b. Loss of cancer drug activity in colon cancer HCT-116 cells during spheroid

- formation in a new 3-D spheroid cell culture system. *Exp Cell Res* 318, 1577–1585. <https://doi.org/10.1016/j.yexcr.2012.03.026>
- Karlsson, H., Senkowski, W., Fryknäs, M., Mansoori, S., Linder, S., Gullbo, J., Larsson, R., Nygren, P., 2019. A novel tumor spheroid model identifies selective enhancement of radiation by an inhibitor of oxidative phosphorylation. *Oncotarget* 10, 5372–5382. <https://doi.org/10.18632/oncotarget.27166>
- Kotsifa, E., Vergadis, C., Vailas, M., Machairas, N., Kykalos, S., Damaskos, C., Garmpis, N., Lianos, G.D., Schizas, D., 2022. Transarterial Chemoembolization for Hepatocellular Carcinoma: Why, When, How? *J Pers Med* 12, 436. <https://doi.org/10.3390/jpm12030436>
- Kung-Chun Chiu, D., Pui-Wah Tse, A., Law, C.-T., Ming-Jing Xu, I., Lee, D., Chen, M., Kit-Ho Lai, R., Wai-Hin Yuen, V., Wing-Sum Cheu, J., Wai-Hung Ho, D., Wong, C.-M., Zhang, H., Oi-Lin Ng, I., Chak-Lui Wong, C., 2019. Hypoxia regulates the mitochondrial activity of hepatocellular carcinoma cells through HIF/HEY1/PINK1 pathway. *Cell Death Dis* 10. <https://doi.org/10.1038/s41419-019-2155-3>
- Li, J., Jiang, E., Wang, X., Shanguan, A.J., Zhang, L., Yu, Z., 2015. Dormant Cells: The Original Cause of Tumor Recurrence and Metastasis. *Cell Biochem Biophys* 72, 317–320. <https://doi.org/10.1007/s12013-014-0477-4>
- Li, X., He, G., Su, F., Chu, Z., Xu, L., Zhang, Y., Zhou, J., Ding, Y., 2020. Regorafenib-loaded poly (lactide-co-glycolide) microspheres designed to improve transarterial chemoembolization therapy for hepatocellular carcinoma. *Asian J Pharm Sci* 15, 739–751. <https://doi.org/10.1016/j.ajps.2020.01.001>
- Li, Y., Gao, Z.-H., Qu, X.-J., 2015. The Adverse Effects of Sorafenib in Patients with Advanced Cancers. *Basic & Clinical Pharmacology & Toxicology* 116, 216–221. <https://doi.org/10.1111/bcpt.12365>
- Lindhagen, E., Nygren, P., Larsson, R., 2008. The fluorometric microculture cytotoxicity assay. *Nat Protoc* 3, 1364–1369. <https://doi.org/10.1038/nprot.2008.114>
- Llovet, J.M., Ricci, S., Mazzaferro, V., Hilgard, P., Gane, E., Blanc, J.-F., de Oliveira, A.C., Santoro, A., Raoul, J.-L., Forner, A., Schwartz, M., Porta, C., Zeuzem, S., Bolondi, L., Greten, T.F., Galle, P.R., Seitz, J.-F., Borbath, I., Häussinger, D., Giannaris, T., Shan, M., Moscovici, M., Voliotis, D., Bruix, J., SHARP Investigators Study Group, 2008. Sorafenib in advanced hepatocellular carcinoma. *N Engl J Med* 359, 378–390. <https://doi.org/10.1056/NEJMoa0708857>
- Lu, J., Tan, M., Cai, Q., 2015. The Warburg effect in tumor progression: mitochondrial oxidative metabolism as an anti-metastasis mechanism. *Cancer Lett* 356, 156–164. <https://doi.org/10.1016/j.canlet.2014.04.001>

- Mahmoud, D.B., Shitu, Z., Mostafa, A., 2020. Drug repurposing of nitazoxanide: can it be an effective therapy for COVID-19? *J Genet Eng Biotechnol* 18, 35. <https://doi.org/10.1186/s43141-020-00055-5>
- Mármol, I., Sánchez-de-Diego, C., Pradilla Dieste, A., Cerrada, E., Rodríguez Yoldi, M.J., 2017. Colorectal Carcinoma: A General Overview and Future Perspectives in Colorectal Cancer. *Int J Mol Sci* 18, E197. <https://doi.org/10.3390/ijms18010197>
- National Center for Biotechnology Information, 2022a. PubChem Compound Summary for CID 11167602, Regorafenib [WWW Document]. National Center for Biotechnology Information. URL <https://pubchem.ncbi.nlm.nih.gov/compound/11167602> (accessed 9.6.22).
- National Center for Biotechnology Information, 2022b. PubChem Compound Summary for CID 216239, Sorafenib [WWW Document]. National Center for Biotechnology Information. URL <https://pubchem.ncbi.nlm.nih.gov/compound/216239> (accessed 9.7.22).
- Nik Nabil, W.N., Xi, Z., Song, Z., Jin, L., Zhang, X.D., Zhou, H., De Souza, P., Dong, Q., Xu, H., 2021. Towards a Framework for Better Understanding of Quiescent Cancer Cells. *Cells* 10, 562. <https://doi.org/10.3390/cells10030562>
- Nygren, P., Larsson, R., 2008. Predictive tests for individualization of pharmacological cancer treatment. *Expert Opinion on Medical Diagnostics* 2, 349–360. <https://doi.org/10.1517/17530059.2.4.349>
- Peng, T.-R., Wu, T.-W., Wu, C.-C., Chang, S.-Y., Chan, C.-Y., Hsu, C.-S., 2022. Transarterial chemoembolization with or without sorafenib for hepatocellular carcinoma: A real-world propensity score-matched study. *Tzu Chi Med J* 34, 219–225. https://doi.org/10.4103/tcmj.tcmj_84_21
- Phan, T.G., Croucher, P.I., 2020. The dormant cancer cell life cycle. *Nat Rev Cancer* 20, 398–411. <https://doi.org/10.1038/s41568-020-0263-0>
- Porporato, P.E., Filigheddu, N., Pedro, J.M.B.-S., Kroemer, G., Galluzzi, L., 2018. Mitochondrial metabolism and cancer. *Cell Res* 28, 265–280. <https://doi.org/10.1038/cr.2017.155>
- Pushpakom, S., Iorio, F., Eyers, P.A., Escott, K.J., Hopper, S., Wells, A., Doig, A., Guilliams, T., Latimer, J., McNamee, C., Norris, A., Sanseau, P., Cavalla, D., Pirmohamed, M., 2019. Drug repurposing: progress, challenges and recommendations. *Nature Reviews Drug Discovery* 18, 41–58. <https://doi.org/10.1038/nrd.2018.168>
- Ren, B., Wang, W., Shen, J., Li, W., Ni, C., Zhu, X., 2019. Transarterial Chemoembolization (TACE) Combined with Sorafenib versus TACE Alone for Unresectable Hepatocellular Carcinoma: A Propensity Score Matching Study. *J Cancer* 10, 1189–1196. <https://doi.org/10.7150/jca.28994>

- Rossignol, J.-F., 2014. Nitazoxanide: a first-in-class broad-spectrum antiviral agent. *Antiviral Res* 110, 94–103. <https://doi.org/10.1016/j.antiviral.2014.07.014>
- Sawicki, T., Ruskowska, M., Danielewicz, A., Niedźwiedzka, E., Arłukowicz, T., Przybyłowicz, K.E., 2021. A Review of Colorectal Cancer in Terms of Epidemiology, Risk Factors, Development, Symptoms and Diagnosis. *Cancers (Basel)* 13, 2025. <https://doi.org/10.3390/cancers13092025>
- Semenza, G.L., 2013. HIF-1 mediates metabolic responses to intratumoral hypoxia and oncogenic mutations. *J Clin Invest* 123, 3664–3671. <https://doi.org/10.1172/JCI67230>
- Senkowski, W., Jarvius, M., Rubin, J., Lengqvist, J., Gustafsson, M.G., Nygren, P., Kultima, K., Larsson, R., Fryknäs, M., 2016. Large-Scale Gene Expression Profiling Platform for Identification of Context-Dependent Drug Responses in Multicellular Tumor Spheroids. *Cell Chem Biol* 23, 1428–1438. <https://doi.org/10.1016/j.chembiol.2016.09.013>
- Senkowski, W., Zhang, X., Olofsson, M.H., Isacson, R., Hoglund, U., Gustafsson, M., Nygren, P., Linder, S., Larsson, R., Fryknas, M., 2015. Three-Dimensional Cell Culture-Based Screening Identifies the Anthelmintic Drug Nitazoxanide as a Candidate for Treatment of Colorectal Cancer. *Molecular Cancer Therapeutics* 14, 1504–1516. <https://doi.org/10.1158/1535-7163.MCT-14-0792>
- Sood, S., Maddiboyina, B., Rawat, P., Garg, A.K., Foudah, A.I., Alam, A., Aldawsari, H.M., Riadi, Y., Singh, S., Kesharwani, P., 2021. Enhancing the solubility of nitazoxanide with solid dispersions technique: formulation, evaluation, and cytotoxicity study. *J Biomater Sci Polym Ed* 32, 477–487. <https://doi.org/10.1080/09205063.2020.1844506>
- Sutherland, R.M., 1988. Cell and environment interactions in tumor microregions: The multicell spheroid model. *Science* 240, 177–184. <https://doi.org/10.1126/science.2451290>
- Tatullo, M., Marrelli, B., Benincasa, C., Aiello, E., Makeeva, I., Zavan, B., Ballini, A., De Vito, D., Spagnuolo, G., 2020. Organoids in Translational Oncology. *J Clin Med* 9. <https://doi.org/10.3390/jcm9092774>
- Types of Cancer Treatment - National Cancer Institute [WWW Document], 2017. URL <https://www.cancer.gov/about-cancer/treatment/types> (accessed 11.20.20).
- Vander Heiden, M.G., Cantley, L.C., Thompson, C.B., 2009. Understanding the Warburg effect: the metabolic requirements of cell proliferation. *Science* 324, 1029–1033. <https://doi.org/10.1126/science.1160809>
- Vaupel, P., Mayer, A., Höckel, M., 2004. Tumor hypoxia and malignant progression. *Methods Enzymol* 381, 335–354. [https://doi.org/10.1016/S0076-6879\(04\)81023-1](https://doi.org/10.1016/S0076-6879(04)81023-1)

- Viale, A., Corti, D., Draetta, G.F., 2015. Tumors and Mitochondrial Respiration: A Neglected Connection. *Cancer Res* 75, 3687–3691. <https://doi.org/10.1158/0008-5472.CAN-15-0491>
- Wells, A., Griffith, L., Wells, J.Z., Taylor, D.P., 2013. The dormancy dilemma: Quiescence versus balanced proliferation. *Cancer Res* 73, 3811–3816. <https://doi.org/10.1158/0008-5472.CAN-13-0356>
- Weng, Z., Luo, Y., Yang, X., Greenhaw, J.J., Li, H., Xie, L., Mattes, W.B., Shi, Q., 2015. Regorafenib impairs mitochondrial functions, activates AMP-activated protein kinase, induces autophagy, and causes rat hepatocyte necrosis. *Toxicology* 327, 10–21. <https://doi.org/10.1016/j.tox.2014.11.002>
- Wenzel, C., Riefke, B., Gründemann, S., Krebs, A., Christian, S., Prinz, F., Osterland, M., Golfier, S., Råse, S., Ansari, N., Esner, M., Bickle, M., Pampaloni, F., Mattheyer, C., Stelzer, E.H., Parczyk, K., Prechtel, S., Steigemann, P., 2014. 3D high-content screening for the identification of compounds that target cells in dormant tumor spheroid regions. *Experimental Cell Research* 323, 131–143. <https://doi.org/10.1016/j.yexcr.2014.01.017>
- What Is Cancer? - National Cancer Institute [WWW Document], 2007. URL <https://www.cancer.gov/about-cancer/understanding/what-is-cancer> (accessed 11.20.20).
- Willis, R., 1934. The Spread of Tumours in the Human Body. *Nature* 1934. <https://doi.org/10.1038/133743c0>
- Wong, C.H., Siah, K.W., Lo, A.W., 2019. Estimation of clinical trial success rates and related parameters. *Biostatistics* 20, 273–286. <https://doi.org/10.1093/biostatistics/kxx069>
- Yang, J.D., Hainaut, P., Gores, G.J., Amadou, A., Plymoth, A., Roberts, L.R., 2019. A global view of hepatocellular carcinoma: trends, risk, prevention and management. *Nature Reviews Gastroenterology & Hepatology* 16, 589–604. <https://doi.org/10.1038/s41575-019-0186-y>
- Zanoni, M., Piccinini, F., Arienti, C., Zamagni, A., Santi, S., Polico, R., Bevilacqua, A., Tesei, A., 2016. 3D tumor spheroid models for in vitro therapeutic screening: a systematic approach to enhance the biological relevance of data obtained. *Sci Rep* 6, 19103. <https://doi.org/10.1038/srep19103>
- Zhang, C., Liu, Z., Bunker, E., Ramirez, A., Lee, S., Peng, Y., Tan, A.-C., Eckhardt, S.G., Chapnick, D.A., Liu, X., 2017. Sorafenib targets the mitochondrial electron transport chain complexes and ATP synthase to activate the PINK1-Parkin pathway and modulate cellular drug response. *J Biol Chem* 292, 15105–15120. <https://doi.org/10.1074/jbc.M117.783175>
- Zhang, J., Salminen, A., Yang, X., Luo, Y., Wu, Q., White, M., Greenhaw, J., Ren, L., Bryant, M., Salminen, W., Papoian, T., Mattes, W., Shi, Q., 2017. Effects of 31 FDA approved small-molecule kinase inhibitors

on isolated rat liver mitochondria. *Arch Toxicol* 91, 2921–2938.
<https://doi.org/10.1007/s00204-016-1918-1>

Zhang, X., De Mito, A., Demiroglu-Zergeroglu, A., Gullbo, J., D’Arcy, P., Linder, S., 2016. Eradicating Quiescent Tumor Cells by Targeting Mitochondrial Bioenergetics. *Trends in Cancer* 2, 657–663.
<https://doi.org/10.1016/j.trecan.2016.10.009>